Contrib Mineral Petrol (2002) 143: 567–586
DOI 10.1007/s00410-002-0356-7

James D. Myers · Bruce D. Marsh · Carol D. Frost
Jennifer A. Linton

Petrologic constraints on the spatial distribution of crustal magma chambers, Atka Volcanic Center, central Aleutian arc

Received: 15 July 2001 / Accepted: 20 January 2002 / Published online: 20 June 2002

Abstract The Atka volcanic center, the largest modern, central Aleutian magmatic complex, covers 360 km^2 with an estimated eruptive volume of ~200 km^3. The oldest exposed rocks, the Old Harbor Series, are a suite of basaltic andesite to dacite flows, pyroclastic rocks and lahars of presumed Tertiary age. The youngest phase of activity on Atka probably began 1–2 Ma ago near the center of the present volcanic field, and consists of basaltic and basaltic andesite flows which produced a large shield volcano, Atka Volcano. Subsequent to this activity, satellite vents formed along the margin of this structure. Collapse of the ancestral Atka Volcano produced a caldera 5 km in diameter and was accompanied by the eruption of a large dacitic flow (Big Pink). After caldera formation, four major volcanic cones (Korovin, Mount Kliuchef, Sarichef and Konia) grew around the margins of Atka caldera. This study focuses on the Atka Volcano, Korovin and Mount Kliuchef volcanic centers. Atka lavas range from basalt through dacite, with all major volcanic vents erupting lavas spanning similar compositional ranges. They are porphyritic with phenocrysts of plagioclase (25–36%), olivine (0.4–3.6%) or orthopyroxene (2.8%), clinopyroxene (1–12%) and a single Fe–Ti oxide (0–2%). Hydrous phases are lacking even in the most evolved lavas. Two generations of plagioclase occur in the Korovin suite but not in lavas from Mount Kliuchef. Korovin plagioclase also displays resorption surfaces and inclusion zones which are either absent in the phenocrysts of Mount Kliuchef lavas or very rare. Similarly, clinopyroxene in Korovin has reaction rims and abundant glass inclusions which are absent in the Mount Kliuchef lavas. Lavas erupted in the Atka volcanic field vary from 47 to 66% SiO_2, although the complex is dominated volumetrically by basaltic lavas. On major-element Harker diagrams, mafic and intermediate Atka Volcano lavas form linear trends but the most siliceous lavas do not fall along these trends. By contrast, Mount Kliuchef lavas are compositionally bimodal whereas Korovin samples range from 51 to 62 wt% silica with intermediate lavas clustering around 55% SiO_2. Incompatible trace-element abundances of Korovin lavas do not increase with silica content but those of Atka Volcano and Mount Kliuchef do. On incompatible-incompatible element diagrams, the three suites behave very differently. Differences also exist between the REE characteristics of the three Atka suites. The petrographic and geochemical differences between the three suites suggest formation by markedly different crustal magmatic processes. The characteristics of the Atka Volcano suite suggest formation of the basalt to dacite suite by crystal fractionation of an anhydrous phenocryst assemblage. Incompatible-incompatible element trends suggest the mafic Mount Kliuchef lavas were also produced by crystal fractionation, a conclusion supported by quantitative mass balance calculations. The difference in slope between the Atka Volcano and Mount Kliuchef suites indicates, however, that there were significant differences in these fractionation schemes. Modeling as well as geochemical characteristics suggest that the Mount Kliuchef dacites are not the product of crystal fractionation. They may represent (1) crustal melts, (2) complete melts of siliceous lava produced during earlier magmatic stages, or (3) residual liquids from the Atka Volcano magmatic system. In contrast to these suites, the Korovin lavas could not have been formed by crystal fractionation. Rather the andesites are probably the result of mixing basaltic and dacitic magmas. The Atka data suggest: (1) large volcanic centers may be supplied by a series of non-communicating, crustal magma chambers; (2) local factors may be important in determining

J.D. Myers (✉) · C.D. Frost · J.A. Linton
Department of Geology and Geophysics,
University of Wyoming,
Laramie, WY 82071, USA
E-mail: magma@uwyo.edu

B.D. Marsh
Department of Earth and Planetary Sciences,
The Johns Hopkins University,
Baltimore, MD 21218, USA

liquid-lines-of-descent; and (3) very different magmatic processes may occur in adjacent magma chambers. If the complexity of the Atka suite is a common feature of arc magmatic plumbing systems, reconstructing differentiation processes requires analytical sample sets which are well constrained spatially and temporally.

Introduction

Subduction zones produce volcanic rocks which display a very wide range of silica contents. Commonly, lavas from individual volcanic centers span the compositional range from basalt to rhyodacite or rhyolite, a silica range of more than 20 wt%. Numerous studies of arc magmatism have suggested that this spectrum of rock types is the product of magmatic processes acting in shallow-level, crustal magma chambers. In the Aleutian arc, petrologic studies have found evidence for the operation of such crustal magmatic processes, such as fractional crystallization (e.g. Perfit et al. 1980; Kay et al. 1983; Baker and Eggler 1987; Singer et al. 1992a, 1992b, 1993), magma mixing (e.g. Conrad et al. 1983; Conrad and Kay 1984; Brophy 1987, 1990) and crustal assimilation (e.g. Brophy 1990; Nye and Turner 1990). Studies of individual arc volcanic centers (Nye and Turner 1990; Brophy 1990; Romick et al. 1990; Singer et al. 1992a, 1992b) also have suggested that there may be temporal and/or tectonic influences on these crustal magmatic processes.

Despite these studies, our understanding of the physical processes operating in the crustal magma chambers of subduction zones remains in its formative stages. Many questions remain as to the nature and scale of these processes. For example, what is the size of individual crustal chambers? Is a given volcanic field with several major volcanic vents supplied by one large magma chamber or does each vent have its own crustal plumbing system? If several magma chambers exist beneath a volcanic center, are they in communication with each other or are they isolated systems? In the latter case, is the same primary magma supplied to the different crustal chambers? In addition to questions of crustal scale, there are also unresolved questions about the influence of local factors on individual liquid-lines-of-descent (LLSDs). For example, do variations in intensive parameters (e.g. temperature, pressure, water content, etc.) produce different LLSDs from the same parental magma? Do the same magmatic processes occur in different chambers simultaneously or can two chambers undergo vastly different processes at the same time? Finally, is there a temporal component to these processes which influences the development of individual magma chambers as well as entire volcanic complexes? These questions can be addressed only by detailed petrologic investigations of large volcanic fields with numerous volcanic vents (e.g. Mount Adams, Hildreth and Lanphere 1994; Tatara-San Pedro complex, Singer et al. 1997; Ruapehu volcano, Nakagawa et al. 1999).

To address some of these fundamental questions, we present new petrographic, geochemical and isotopic results from the Aleutian volcanic center of Atka. This center is ideal for such a study because it records, within a relatively limited geographic area, the magmatic activity of several volcanic vents (Marsh 1980). Previous reconnaissance surveys (Marsh 1980; Myers et al. 1985, 1986) have also shown that these volcanic vents have erupted a broad compositional spectrum of lavas. By combining earlier work with our new petrographic, geochemical and isotopic data, the liquid-lines-of-descent for several of the major volcanic vents in the Atka volcanic complex (Atka Volcano, Korovin and Mount Kliuchef) have been characterized more fully. This combination of data permits identification of intra-center compositional variations and evaluation of magmatic evolution at crustal levels in subduction settings.

Regional setting

In the central and western Aleutian arc, the modern volcanic centers are the subaerial expressions of a ridge massif which rests upon oceanic crust and lithosphere presumably of Cretaceous age (Cooper et al. 1975; Scholl et al. 1987; Geist et al. 1987, 1988). Based on seismic and bathymetric data, Geist et al. (1988) postulated that this massif has been fragmented into five major crustal blocks (Fig. 1a). From east to west these blocks are Andreanof, Delarof, Rat, Buldir and Near. Five modern volcanic centers occur along the northern margin of the Andreanof block (Fig. 1b). The five centers, Seguam, Atka, Great Sitkin, Adak and Kanaga, differ geologically (Singer and Myers 1990). The modern volcanic field on Kanaga is a circular volcanic complex covering 75 km^2 with five major vents (Coats 1952). On Adak, the modern magmatic phase was centered around three volcanic vents located in a 100-km^2 area (Coats 1952; Myers and Frost 1994). Great Sitkin, immediately to the east of Adak (Fig. 1b), is a large, composite volcano with two major central vents (Simons and Mathewson 1955). It covers an area ($\sim$250 km^2) nearly two and a half times greater than Adak. The largest of the Andreanof volcanic centers (360 km^2) is Atka, which is dominated volumetrically by mafic lavas. It consists of a large shield volcano capped by small andesitic and dacitic vents. Seguam, located approximately 100 km east of Atka, is unusual in that its six major volcanic vents are aligned in an east-west orientation (Singer et al. 1992a, 1992b).

General geology

Atka, one of the active islands of the Andreanof group (Fig. 1b), consists of two geographically distinct parts. In the southwestern portion of the island, metamorphic

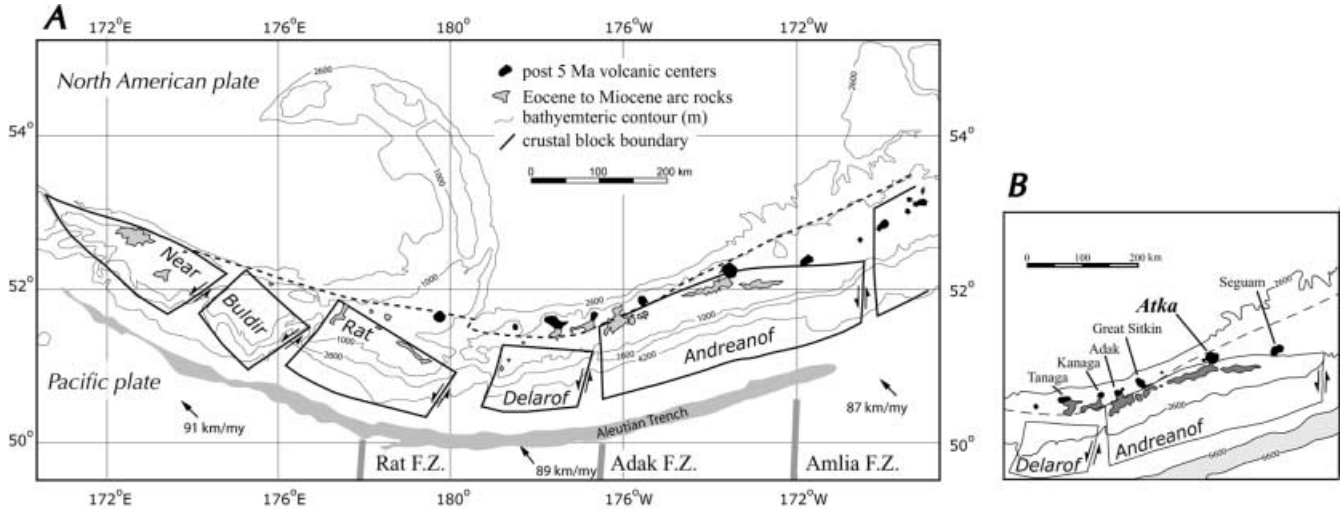

Fig. 1a, b. Map showing the tectonic and structural setting of the central Aleutian arc. **a** Because of the oblique subduction of the Pacific plate beneath the North American, the arc massif has been fragmented into five crustal blocks, from east to west: Andreanof, Delarof, Rat, Buldir and Near. **b** Five modern volcanic centers occur along the northern margin of the Andreanof block. From east to west, these centers are Seguam, Atka, Great Sitkin, Adak and Kanaga. Of these, Atka is the largest

rocks are exposed in low, rounded hills (Hein et al. 1984). Northeastern Atka is formed of young volcanic rocks which have been transformed into a rugged terrain by a combination of volcanic and glacial activity. This portion of the island covers 360 km^2 with an estimated eruptive volume of 200 km^3 (Fig. 2; Marsh 1980). The tallest peak, Korovin, is 1,530 m high and located along the northern coast. Mount Kliuchef is the second highest peak, situated nearly in the center of the volcanic field and has an elevation of 1,460 m. It is ringed by a series of peaks ranging in height from 748 m to 1,433 m.

The volcanic rocks exposed on northeastern Atka record the growth of at least two major shield volcanoes and their satellite vents, the formation of a large caldera, and the creation of four post-caldera volcanoes (Marsh 1980). The oldest volcanic products are a series of basaltic andesite to dacite flows, pyroclastic rocks and lahars found around the margin of Korovin Bay (Fig. 2). These rocks, the Old Harbor Volcanics, presumably represent the remnants of a large shield volcano formerly located in Korovin Bay. A preliminary K–Ar date on a plug from this formation yielded an age of 6.6 Ma (Marsh 1982). This shield volcano and its associated volcanic rocks are Tertiary in age and presumably predate the modern magmatic phase of the Aleutian arc.

The youngest phase of volcanism on Atka probably began one to two million years ago and was concentrated around the approximate center of the present volcanic field (Fig. 2). Initial volcanic activity consisted of the eruption of a large number of basalt and basaltic andesite flows. These flows vary in thickness from 1 to 2 m and in some places can be traced laterally for up to 2 km in sea cliffs and the walls of glacial valleys. The large basaltic shield produced by this activity is composed almost exclusively of basalts and basaltic andesites with few pyroclastic units. It probably had an original basal diameter of at least 20 km and a minimum subaerial thickness of 100 m at the volcano margin (Myers et al. 1986). Subsequent glacial activity produced large valleys cutting this shield which are radially distributed around the center of the island.

After this initial activity, the central cone, Atka Volcano, grew on top of the shield and probably reached an elevation of ~2,200 m. A series of satellite vents then formed, ringing the central cone (Fig. 2). These volcanic edifices are comprised of lava flows as well as pyroclastic units including many lahars. The increase in the abundance of pyroclastic rocks as well as the change in the dominant lava from basalt to andesite differentiates these later volcanic vents from the earlier, shield building stage. Summit glaciers have breached many of the summit craters, thereby forming active cirques which dissect many of the satellite vents. Ancestral Atka Volcano subsequently collapsed, creating a caldera 5 km in diameter (Fig. 2). Associated with this event was the eruption of a large dacitic flow (Fig. 3). This flow, called Big Pink because of its distinctive field appearance, is approximately 400 m thick, nearly oval in outline and 2–3 km in maximum dimension (Fig. 2). It consists of pumiceous and glassy units but is not associated with any ash flows. A hydration date from Big Pink suggests the caldera-forming eruption of ancestral Atka Volcano occurred 300,000 to 500,000 years ago (Marsh, unpublished data). A series of NW-trending dikes cuts the entire Atka Volcano shield and was presumably emplaced during caldera formation (Fig. 2). The dikes are nearly vertical and approximately 1 m thick.

After collapse, four major volcanic cones grew around the margins of Atka caldera: Mount Kliuchef, Korovin Volcano, Konia and Sarichef. Mount Kliuchef occurs along the western rim of Atka caldera in the center of the volcanic field, and it is marked by a series of five fumaroles (Fig. 2). It is 1,460 m high and topped by a double summit with two small lakes. Kliuchef is

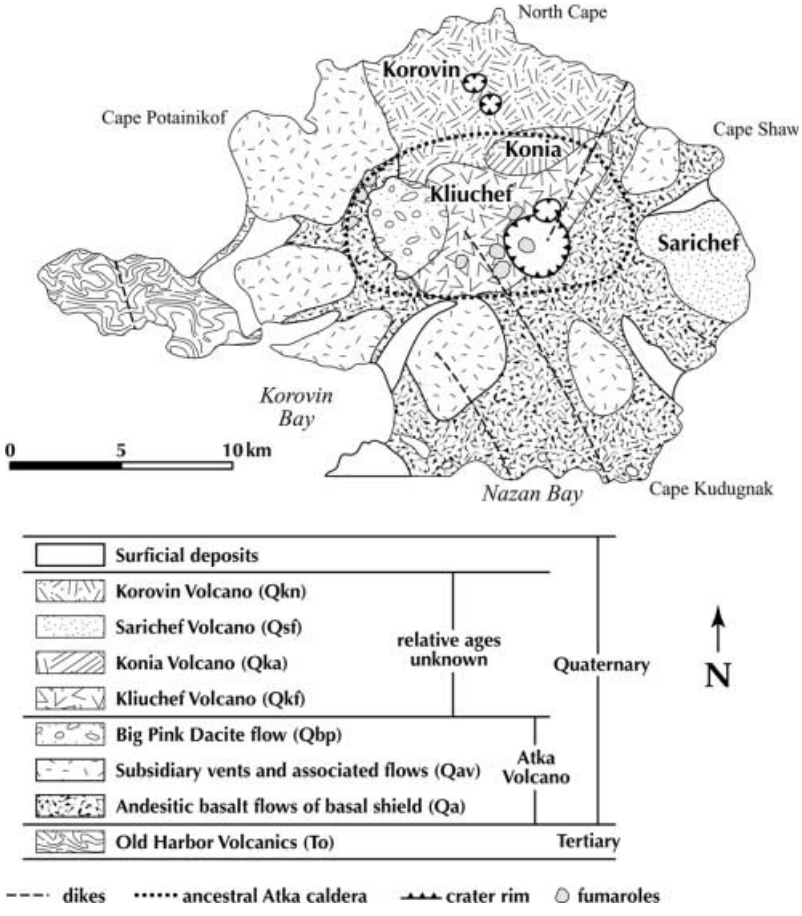

Fig. 2. Generalized geologic map of northeastern Atka Island. The oldest volcanic products are the Old Harbor Volcanics which are exposed around Korovin Bay. A preliminary K–Ar date suggests they are Tertiary in age (Marsh 1982). This pile of flows, stocks, dikes and pyroclastic units is interpreted as the remnants of a large volcano formerly located in the present Korovin Bay. Recent volcanic activity at Atka produced the ancestral Atka Volcano, a large stratovolcano ringed by at least three satellite vents all superimposed on a large basal shield. This volcano was destroyed by an eruption which produced a caldera 5 km in diameter (*dotted line*). At this time, a large dacite flow, Big Pink, was erupted on the caldera floor. A hydration date from this flow suggests this event occurred 300,000 to 500,000 years ago. Subsequent to caldera formation, four volcanoes (Korovin, Mount Kliuchef, Konia and Sarichef) were produced within Atka caldera or on the flanks of the ancestral volcano. The relative timing of these volcanoes is unknown (after unpublished map of B.D. Marsh)

composed of basalt to dacite flows with a large number of intercalated pyroclastic rocks, autobreccias and lahars. Glassy dacite flows occupy most of Kliuchef's summit area. The summit has been sculpted by glacial ice and the lower southeastern flank is partly covered by an ice field. Three hot springs and fumerolic areas occur on the southern and western flanks of Kliuchef (Fig. 2; Motyka et al. 1981).

Located about 5 km north of Mount Kliuchef, Korovin Volcano, with an elevation of 1,553 m and a basal diameter of 7 km, is the largest and tallest of the post-caldera volcanoes. Unlike Mount Kliuchef, this edifice shows little evidence of glaciation and does not presently support glaciers, even though it is the taller of the two volcanoes. Its uneroded form suggests the volcano is mostly Holocene in age. Korovin is a double cone, with the two summits 0.6 km apart. The NW summit is the lower of the two and is a symmetric cone with a small crater. The SE summit is higher with a steep-walled crater. The crater is about 1 km wide at the top and several hundred meters deep. The walls of the top portion of the crater consist of intercalated lava flows and pyroclastic rocks. By contrast, the bottom hundred meters or so consists of vertical walls almost exclusively of lava flows. A small active geothermal field occurs at the head of a glacial valley 6.5 km SW of Korovin (Motyka et al. 1981). Historic volcanic activity has been reported in 1829, 1844, 1907, 1951, 1953, 1973, 1976, and 1986 (Simkin and Siebert 1994; Miller et al. 1998). Satellite images recorded the most recent volcanic

Fig. 3. Photograph of the Big Pink dacite flow (middle ground). This unit was erupted on the floor of Atka caldera and is approximately 750 m thick, oval in outline and 2 to 3 km in maximum dimension. Its name is derived from its distinctive appearance in the field. The scarp visible to the right of Big Pink is part of the margin of Atka caldera. Behind the dacite flow is Korovin Bay, the site of a former Tertiary shield volcano. Rocks of the Old Harbor Series are exposed in the shoreline around the bay (photograph by J.D. Myers)

activity from Korovin on 18 March 1987 when three plumes were observed drifting from Korovin and several Kliuchef vents (Miller et al. 1998).

Konia, a small post-caldera cone, lies in the high saddle between these two volcanoes. A fresh cinder cone occurs on the western flank of this volcano. The late-stage eruptive products of Korovin and Konia are glassy dacite lava flows. The fourth post-caldera volcano, Sarichef, is located on the eastern margin of the island and grew on the flanks of the ancestral Atka Volcano (Fig. 2). This volcano is symmetrical in shape and nearly undissected. Although an 1812 eruption is attributed to Sarichef (Coats 1950), field evidence for such a recent eruption is lacking.

Because few samples from Atka have been dated, the temporal evolution of this large volcanic center is based on geologic relations. Bingham and Stone (1972) report K–Ar ages for basalts from Korovin Volcano. Given the errors of these results, the shield must be older than 600,000 years. Because they are isolated spatially, the relative ages of the four post-caldera cones are uncertain. Marsh (1990) suggests Korovin formed after Mount Kliuchef but that significant overlap occurred. Based on the degree of dissection, Marsh (1982, and unpublished data) suggested the latest stage of volcanism which produced the post-caldera events occurred about 100,000 years ago.

Previous work

Early geologic investigations of northeastern Atka were limited in scope. In 1873, W.M. Dall and M. Baker of the US Coast Survey climbed to the geothermal springs in the valley between Korovin and Mount Kliuchef and measured the temperature of the spring water (Dall 1918). Motyka et al. (1981) subsequently performed a modern investigation of this geothermal area as well as the one on Mount Kliuchef. Another early field investigation of northeastern Atka was conducted by T.A. Jagger in 1907. The only report resulting from this expedition was a journal article with few scientific results but which amply illustrates the difficulties associated with fieldwork in the Aleutian arc (Jagger 1908). A geologic report on this volcanic center was not included as part of the 1945–1954 U.S. Geological Survey investigation of Alaskan volcanoes. As part of their paleomagnetic survey of the Aleutian arc, Bingham and Stone (1972) dated by K–Ar several cores from a basalt from Korovin Volcano. Kay and Kay (1994) report major-, trace- and rare-earth element data for a sample from northeastern Atka but do not describe its geologic setting. Aside from these reconnaissance surveys, northeastern Atka Island has been the subject of only two, systematic mapping programs. The first was by R.E. Leitz and B.D. Marsh in 1973. This effort was followed by two field seasons in 1976 and 1977 by Marsh assisted by J.D. Myers. Preliminary geochemical data from the Atka volcanic suite have been published by Marsh (1980), Myers et al. (1985, 1986), Myers and Marsh (1987), and Myers and Frost (1989). These studies included samples which spanned the compositional range of the entire volcanic suite but did not differentiate data according to volcanic vent. Baker and Eggler (1983, 1987) conducted experimental studies on a number of Atka samples. The present study reports new major-, trace- and rare-earth element well as Sr, Nd and Pb isotopic results. When combined with previously published data, analyzed suites covering the entire compositional spectrums of two of the major Atka volcanoes, Korovin and Mount Kliuchef, are available. This more complete data set allows identification of geochemical differences between the volcanic vents as well as documentation of compositional shifts over the duration of the entire volcanic complex.

Analytical procedures

Mineral compositions and zoning patterns were determined using the University of Wyoming's automated Cameca MBX electron microprobe (Tables 1, 2, 3). Natural mineral standards compositionally similar to the unknowns were used for calibration. Plagioclase analyses were performed with an accelerating potential of 15 kV, 10-s counting times, a ≤ 5 μm beam spot and a 10-nA beam current. Mafic phases, i.e., olivine and pyroxenes, were analyzed with similar operating conditions except that a beam current of 20 nA was used. Matrix corrections were performed using a ZAF procedure. After calibration for each analysis session, standardization was checked by analyzing mineral standards not utilized in the original calibration. Plagioclase compositional profiles were defined by running automated line scans beginning in a crystal's core and proceeding to its rim. Individual analysis points were spaced approximately 20 μm apart. Line scans were performed only on the largest mafic crystals. Zoning within smaller phenocrysts was defined by analyzing cores and rims.

Major-element compositions for 23 Atka lavas are reported in Table 4. These samples span the compositional ranges characteristic of Atka Volcano as well as the post-caldera cones of Korovin and Mount Kliuchef. Of these analyses, 13 are new and were done wet chemically at the University of Leeds. Ferrous iron contents were determined by titration at Johns Hopkins University. The remaining major-element analyses have been reported previously by Myers et al. (1985, 1986). Additional major-element analyses of basaltic lavas from the shield of Atka Volcano are given by Myers et al. (1986), and Kay and Kay (1994) report the composition of an andesite presumably from Korovin.

Trace-element contents of 17 samples are also reported in Table 4. Of these, Rb, Sr and Ba contents have been previously reported for six samples (Myers et al. 1985). The new analyses were performed by DCP-AES at Rutgers University on samples analyzed previously for major elements, selected trace elements, and Sr and Pb isotopic compositions (Myers et al. 1985; Myers and Marsh 1987). For trace elements, 0.2 g sample was fused with 0.7 g $LiBO_2$ and the resultant beads dissolved in 50 ml 5% HCl. Approximately 0.2 g sample was fused with 0.5 g flux and dissolved in 25 ml 1.5 N HCl for rare-earth element determinations. Except for one sample, agreement between the new results and the earlier work averages 2% for Sr. Ba differences are slightly greater (5–10%), with the DCP results generally lower. Because of the similarity of our new results with those previously reported and for internal consistency, Sr and Ba contents from the present study are reported in Table 4. Trace-element duplicate analyses of samples and internal standards generally agreed within 5% for all elements.

Rare-earth element abundances and Sr, Nd and Pb isotopic results for 17 samples are reported in Table 5. The rare-earth elements were separated and concentrated for analysis using the

Table 1. Representative average plagioclase compositions

	Atka	Mount Kliuchef					Korovin		
	AT-112	AT-53	AT-94	AT-90	AT-57	AT-88	AT-52	AT-48	AT-49
Oxide (wt%)									
SiO_2	47.55	48.62	55.40	54.04	51.90	60.20	49.76	52.67	52.24
Al_2O_3	32.90	33.08	27.91	29.06	29.29	26.03	31.10	30.16	30.07
Fe_2O_3	0.96	0.99	0.83	0.76	0.92	0.40	1.02	0.87	0.68
CaO	16.25	16.12	10.87	11.68	13.18	6.72	14.96	12.50	13.30
Na_2O	2.37	2.40	5.06	4.70	4.28	6.82	2.87	4.57	4.17
K_2O	0.13	0.12	0.72	0.46	0.23	0.72	0.19	0.39	0.27
Total	100.16	101.33	100.79	100.70	99.80	100.89	99.90	101.16	100.73
Element	Stoichiometric proportions based on 8 oxygens								
Si	2.1843	2.2035	2.4885	2.4331	2.3719	2.6584	2.2798	2.3708	2.3625
Al (IV)	1.7817	1.7673	1.4779	1.5422	1.5781	1.3555	1.6801	1.6004	1.6035
Tetrahedral	3.9660	3.9708	3.9664	3.9753	3.9500	4.0139	3.9599	3.9712	3.9660
Fe	0.0330	0.0337	0.0280	0.0258	0.0316	0.0133	0.0352	0.0295	0.0231
Ca	0.8000	0.7827	0.5233	0.5635	0.6454	0.3180	0.7343	0.6030	0.6444
Na	0.2113	0.2105	0.4407	0.4103	0.3793	0.5836	0.2553	0.3987	0.3659
K	0.0075	0.0070	0.0412	0.0264	0.0134	0.0404	0.0111	0.0221	0.0156
Octahedral	1.0518	1.0339	1.0332	1.0260	1.0697	0.9553	1.0359	1.0533	1.0490
	End-member proportions								
An	78.5	78.3	52.1	56.3	62.2	33.8	73.4	58.9	62.8
Ab	20.7	21.0	43.8	41.0	36.5	62.0	25.5	38.9	35.7
Or	0.7	0.7	4.1	2.6	1.3	4.3	1.1	2.2	1.5
Total	99.9	100.0	100.0	99.9	100.0	100.1	100.0	100.0	100.0

Table 2. Representative average olivine compositions

	Atka	Mount Kliuchef				Korovin		
	AT-112	AT-53	AT-94	AT-90	AT-57	AT-52	AT-48	AT-49
Oxide (wt%)								
SiO_2	36.42	35.51	36.12	35.59	34.45	36.79	36.25	35.16
FeO	30.21	30.54	34.44	33.06	33.52	30.20	27.25	29.35
MnO	0.50	0.68	0.74	0.72	0.78	0.58	0.57	0.48
NiO	0.06	0.01	0.06	–	0.05	–	0.02	0.06
MgO	33.87	33.21	28.62	31.30	30.81	32.48	34.89	34.27
CaO	0.22	0.31	0.24	0.24	0.24	0.21	0.17	0.16
Total	101.28	100.26	100.22	100.91	99.85	100.26	99.15	99.48
Element	Stoichiometric proportions based on 4 oxygens							
Si (IV)	0.9758	0.9665	0.9991	0.9727	0.9582	0.9946	0.9799	0.9595
Fe	0.6769	0.6952	0.7967	0.7559	0.7798	0.6828	0.6160	0.6699
Mn	0.0115	0.0156	0.0173	0.0168	0.0185	0.0133	0.0132	0.0111
Ni	0.0013	0.0001	0.0012	–	0.0011	0.0001	0.0005	0.0013
Mg	1.3525	1.3470	1.1796	1.2749	1.2770	1.3085	1.4057	1.3939
Ca	0.0064	0.0090	0.0070	0.0071	0.0072	0.0061	0.0048	0.0047
Octahedral	2.0486	2.0669	2.0018	2.0547	2.0836	2.0108	2.0402	2.0809
	End-member proportions							
Fo	66.4	65.7	59.5	62.6	61.9	65.5	69.4	67.4
Fa	33.3	33.9	40.2	37.1	37.8	34.2	30.4	32.4
Mg#	66.6	66.0	59.7	62.8	62.1	65.7	69.5	67.5

column-exchange procedures of Feigenson and Carr (1985) and measured by DCP-AES. Rare-earth element duplicates run during this study agree within 2–3%.

Strontium isotopic ratios for 23 Atka lavas have been previously reported by Myers et al. (1985, 1986) and von Drach et al. (1986). Myers and Marsh (1987) also reported Pb isotopic compositions for 12 samples from Atka. The additional Sr and Pb as well as the new Nd isotopic ratios reported in Table 5 were measured at the University of Wyoming using a VG Sector mass spectrometer. Approximately 50 mg powder were dissolved in HF and HNO_3, split and spiked, and Sr, Pb and Nd extracted using standard ion-exchange procedures (Winchester 1963; Hooker et al. 1975). Early in this investigation, six Nd isotopic ratios were measured using a VG Sector single-collector mass spectrometer whereas samples analyzed later were run on a VG Sector multi-collector mass spectrometer. Normalizing values were $^{146}Nd/^{144}Nd = 0.7219$ and $^{86}Sr/^{88}Sr = 0.1194$. Total chemistry blanks were less than 50 pg for Nd and less than 200 pg for Sr. On the University of Wyoming mass spectrometers, the $^{143}Nd/^{144}Nd$ ratio for the La Jolla standard is 0.511846 (s.d. $= 5.2\times10^{-6}$) and the $^{87}Sr/^{86}Sr$ ratio for NBS987 is 0.710246 (s.d. $= 1.2\times10^{-5}$). Nd and Sm concentrations determined by isotope dilution are reported only when DCP measurements are unavailable. Two-sigma uncertainties for Pb isotopic ratios were less than 0.5%. Measured isotopic Pb ratios were corrected by a mass fractionation factor of $0.10 \pm 0.04\%$ per amu as determined by runs of NBS981.

Table 3. Representative average clinopyroxene compositions

	Atka	Mount Kliuchef					Korovin		
	AT-112	AT-53	AT-94	AT-90	AT-57	AT-88	AT-52	AT-48	AT-49
Oxide (wt%)									
SiO_2	50.27	50.80	50.54	52.02	50.85	51.55	51.32	52.82	52.20
TiO_2	0.78	0.58	0.68	0.48	0.59	0.35	0.51	0.45	0.37
Al_2O_3	3.84	3.78	3.09	2.56	2.88	1.41	2.43	2.65	2.94
FeO	11.55	7.92	13.03	9.04	11.11	13.19	9.95	10.11	7.65
MnO	0.34	0.19	0.47	0.38	0.38	0.80	0.35	0.59	0.24
MgO	14.66	15.20	15.19	15.53	16.27	13.76	15.30	14.84	16.03
CaO	18.81	21.13	16.25	20.23	18.92	19.19	19.22	19.28	20.57
Na_2O	0.33	0.34	0.46	0.30	0.49	0.21	0.30	0.35	0.23
Total	100.58	99.94	99.71	100.54	101.49	100.46	99.38	101.09	100.23
Element	Stoichiometric proportions based on 6 oxygens								
Si	1.862	1.874	1.891	1.915	1.860	1.935	1.916	1.943	1.917
Ti	0.022	0.016	0.019	0.013	0.016	0.010	0.014	0.012	0.010
Al	0.168	0.164	0.136	0.111	0.124	0.062	0.107	0.115	0.127
Fe^{+3} [a]	0.088	0.080	0.078	0.055	0.126	0.058	0.055	–	0.035
Fe^{+2}	0.270	0.165	0.330	0.224	0.213	0.356	0.256	0.311	0.200
Mn	0.011	0.006	0.015	0.012	0.012	0.025	0.011	0.018	0.007
Mg	0.809	0.836	0.847	0.852	0.887	0.770	0.851	0.814	0.877
Ca	0.747	0.835	0.651	0.798	0.742	0.772	0.769	0.760	0.809
Na	0.024	0.024	0.033	0.021	0.035	0.015	0.022	0.025	0.016
Sum	4.001	4.000	4.000	4.001	4.015	4.003	4.001	3.998	3.998
	End-member proportions								
En	44.3	45.5	46.3	45.5	48.2	40.6	45.4	43.2	46.5
Fs	14.8	9.0	18.0	11.9	11.6	18.8	13.6	16.5	10.6
Wo	40.9	45.5	35.6	42.6	40.3	40.7	46.0	40.3	42.9

[a] Fe^{+3} calculated according to Lindsley and Anderson (1983)

Petrography and mineral compositions

Atka lavas are porphyritic with phenocrysts of plagioclase, olivine, clinopyroxene, orthopyroxene and a single Fe–Ti oxide. Hydrous phases are lacking even in the most evolved samples. Plagioclase is the dominant phase in all samples and the opaque phases occur only as microphenocrysts. Individual plagioclase phenocrysts range in size continuously from microphenocrysts (400 μm) to nearly 2 mm in maximum dimension. Unlike plagioclase and the oxide phase, the dominant ferromagnesian phase varies with silica content. Olivine and/or clinopyroxene occur in the basalts and basaltic andesites but orthopyroxene replaces olivine as the mafic phase in the most siliceous samples. Clinopyroxene phenocrysts range in size from 0.3 to 1.0 mm in maximum dimension and occur mostly in glomerocrysts. Olivine phenocrysts generally occur as isolated crystals and are smaller (0.1–0.3 mm) than clinopyroxene crystals. In general, total phenocryst contents are highest in the most mafic lavas and lowest in the more evolved dacites (Table 4). Groundmass phases consist of the same mineral assemblage as those characteristic of the phenocrysts plus small amounts of glass. A detailed petrographic study of plagioclase compositions and zoning in lavas from Mount Kliuchef and Korovin has been reported by Linton (1993) and Linton et al. (1993).

Atka Volcano

A basalt typifying the base of Atka Volcano, collected from Nazan Bay, contains phenocrysts of plagioclase, olivine and clinopyroxene. The average composition of individual plagioclase phenocrysts varies from An_{70} to An_{86} (Table 1), with no simple correlation between crystal size and composition. Microphenocrysts (<400 μm) span a slightly greater range ($An_{69–86}$) but overlap the phenocrysts compositionally ($An_{70–84}$). Groundmass plagioclase crystals are considerably more sodic ($<An_{69}$) than phenocrysts or microphenocrysts and do not compositionally overlap the phenocrysts (Fig. 4). Olivine crystals range in average composition from 63 to 70 mol% Fo (Table 2) and are unzoned. Coexisting clinopyroxene crystals are also relatively iron-rich (Table 3), with little compositional variability (Fig. 4).

Korovin Volcano

Korovin samples contain 1–12% clinopyroxene, 0.4–3.6% olivine, 25–32% plagioclase, and 0–2% oxides. Average plagioclase compositions vary from An_{58} to An_{88} in basalts, and from An_{47} to An_{74} in andesites. There is no simple correlation between phenocryst composition and silica content (Fig. 5). Within individual samples, phenocryst compositions vary by nearly

Table 4. Major- and trace-element compositions of Atka lavas. *AV* Atka Volcano, *KFV* Mount Kliuchef Volcano, *KNV* Korovin Volcano

Volcano	AV	AV	AV	AV	AV	AV	AV	AV	KFV	KFV	KFV	KFV	KFV	KFV	KFV	KFV	KFV	KFV	KFV	KNV	KNV	KNV	KNV	2σ error
Map unit	Qa	Qa	Qa	Qa	Qav	Qav	Qav	Qbp	Qkf	Qkf	Qkf	Qkf	Qkf	Qkf	Qkf	Qkf	Qkf	Qkf	Qkf	Qkn	Qkn	Qkn	Qkn	
Sample #	AT-112	AT-71[a]	AT-73[a]	AT-76[a]	AT-21[b]	AT-34[b]	AT-22[b]	AT-121[b]	AT-53	AT-56	AT-94	AT-89	AT-90[b]	AT-92	AT-93	AT-91	AT-57	AT-118	AT-88	AT-52	AT-48	AT-49	AT-117[b]	
SiO_2	47.81	49.07	49.08	50.42	55.70	58.24	61.37	66.77	51.20	52.00	52.60	52.70	53.10	53.20	53.50	53.60	55.30	66.03	66.70	51.50	55.90	56.10	62.49	0.62
TiO_2	0.82	0.88	0.89	0.92	0.98	0.69	0.84	0.44	0.96	0.91	1.04	1.02	1.08	1.01	1.04	1.04	1.04	0.46	0.54	0.99	0.84	0.82	0.62	0.03
Al_2O_3	19.90	20.13	20.36	20.59	18.58	17.33	16.09	16.41	18.90	19.50	18.30	19.10	17.60	18.60	18.60	18.40	18.70	16.12	16.40	18.10	16.60	17.30	16.37	0.13
Fe_2O_3	–	3.42	3.80	4.32	4.21	3.91	4.03	2.01	4.05	4.65	3.06	4.08	3.36	–	3.69	4.30	3.78	–	1.56	3.67	2.18	3.23	1.99	–
FeO	–	6.46	5.39	5.28	3.81	3.25	2.39	0.87	5.63	5.27	6.43	5.60	6.43	–	6.22	5.31	4.86	–	2.96	6.15	5.66	4.34	3.95	–
FeO^t	9.49	9.54	8.81	9.17	7.60	6.77	6.02	2.68	9.27	9.45	9.18	9.27	9.45	9.09	9.54	9.18	8.26	4.16	4.36	9.45	7.62	7.25	5.74	–
MnO	0.18	0.19	0.18	0.18	0.18	0.16	0.13	0.04	0.20	0.25	0.20	0.18	0.20	0.14	0.21	0.18	0.16	0.13	0.17	0.13	0.14	0.18	0.15	0.00
MgO	6.21	4.27	3.39	3.49	1.87	3.24	1.70	0.15	5.29	4.61	4.05	3.94	3.81	3.83	3.35	3.47	3.07	0.64	0.94	5.00	4.27	3.82	1.69	0.10
CaO	11.08	9.80	9.93	10.27	7.41	7.10	4.10	1.64	9.87	10.10	8.82	8.82	8.71	8.55	7.44	8.88	8.11	2.36	2.76	9.73	8.37	7.30	4.23	0.07
Na_2O	2.79	3.19	3.25	3.27	4.12	3.74	4.50	4.46	3.00	3.27	3.23	3.54	3.89	3.79	3.89	3.09	3.79	4.74	5.13	3.21	3.71	3.60	4.53	0.10
K_2O	0.63	0.68	0.71	0.70	1.82	2.00	2.97	4.18	0.74	0.62	1.10	0.80	1.12	1.18	1.28	1.20	1.54	4.60	3.68	1.08	1.90	1.77	3.00	0.09
P_2O_5	0.18	0.15	0.16	0.13	0.30	0.19	0.37	0.12	0.19	0.24	0.23	0.29	0.27	0.27	0.28	0.30	0.49	0.15	0.18	0.22	0.18	0.18	0.19	0.01
H_2O^+/LOI	–	–	–	–	1.05	0.34	1.46	2.14	–	–	–	–	–	–	–	–	–	–	–	–	–	–	0.14	–
H_2O^-	–	–	–	–	–	0.10	–	–	–	–	–	–	–	–	–	–	–	–	–	–	–	–	0.07	–
Total	99.09	98.24	97.14	99.57	100.03	100.29	99.95	99.23	100.03	101.42	99.06	100.07	99.57	99.66	99.50	99.77	100.84	99.39	101.02	99.78	99.75	98.64	99.42	–
Rb	–	8	9	8	40.2	41.3	78.3	115.4	–	–	–	–	22.7	–	–	–		–	–	–	–	–	34	–
Sr	562	637	645	661	474	482	339	154	541	–	504	–	517	–	–	–	453	–	210	481	544	457	469	21
Y	16.2		18.7	15.5	31.1	18.8	35.0	57.0	21.6	–	27.4	–	30.5	–	–	–	38.1	–	47.2	23.9	29.0	30.4	31.4	2
Zr	53	48	50	50	129	128	215	293	59	–	90	–	103	–	–	–	143	–	271	90	81	144	146	30
Ba	299	310	317	321	521	737	747	902	329	–	379	–	446	–	–	–	553	–	889	429	597	537	565	31
Sc	34	26	23	25	23	17	15	8	29	–	31	–	29	–	–	–	25	–	12	33	26	27	23	1
V	309	253	268	277	201	146	88	24	289	–	285	–	250	–	–	–	189	–	49	286	182	223	216	22
Cr	27	99	90	13	6	32	3	3	26	–	35	–	10	–	–	–	24	–	6	44	182	38	10	17
Ni	23	57	54	15	6	16	2	2	25	–	23	–	8	–	–	–	17	–	3	33	44	18	17	8
Cu	130	131	92	114	46	39	30	13	110	–	132	–	132	–	–	–	139	–	35	108	219	38	99	–
Modal proportions of phenocyrst phases																								
Plag	42.9	34.9	34.1	34.6	24.6	2.94	5.5	–	22.6	27.6	26.2	20.5	13.9	16.6	19.2	20.6	19.7	13.9	15.9	20.9	24.1	28.6	–	
Olivine	7.4	3.7	2.8	0.9	0.2	0.5	–	–	3.4	6.4	1.4	1.2	1.6	1.1	2.6	0.1	1.7	–	–	2.5	0.5	1.2	–	
Epx	0.25	–	–	–	0.7	6.7	0.4	–	2.4	2.4	4.1	0.6	3	1.5	1.5	1.2	0.9	1.1	1.7	2.4	7.6	7.5	–	
Opx	–	–	–	–	–	0.5	0.1	–	–	–	–	–	–	–	–	–	–	–	–	–	–	–	–	
Opaques	–	0.7	0.2	–	0.5	1.4	–	–	–	1.8	0.1	0.2	0.4	–	0.7	0.4	0.5	1	1	0.1	1.4	1.9	–	

[a]Major elements from Myers et al. (1986)
[b]Major elements and Rb contents from Myers et al. (1985). Sr and Ba contents are new but within error of previously reported values. Major-element totals calculated using FeO^t

Table 5. Rare-earth element and Sr, Nd and Pb isotopic compositions of Atka lavas. *AV* Atka Volcano, *KFV* Mount Kliuchef Volcano, *KNV* Korovin Volcano

Volcano	AV	AV	AV	AV	AV	AV	AV	KFV	KFV	KFV	KFV	KFV	KNV	KNV	KNV
Map unit	Qa	Qa	Qa	Qav	Qav	Qav	Qbp	Qkf	Qkf	Qkf	Qkf	Qkn	Qkn	Qkn	Qkn
Sample #	AT-12	AT-71[a]	AT-73	AT-76	AT-21	AT-34[b, c]	AT-22	AT-121[b, c]	AT-53	AT-94	AT-90[b, c]	AT-57	AT-88	AT-52	AT-48	AT-49	AT-117[b, c]
SiO_2	47.81	49.07	49.08	50.42	55.70	58.24	61.37	66.77	51.20	52.60	53.10	55.30	66.70	51.50	55.90	56.10	62.49
La	5.4	–	6.4	5.0	12.7	10.0	17.7	20.0	7.51	9.85	12.1	15.2	22.2	8.54	11.9	12.3	14.2
Ce	12.59	–	15.7	12.9	31.3	23.3	43.3	53.3	17.4	22.9	27.3	35.0	52.8	20.4	27.9	29.7	31.9
Nd	8.76	13.96[d]	10.8	8.2	19.0	12.4	24.9	26.5	13.2	16.5	18.8	24.9	28.1	14.6	18.0	19.3	18.6
Sm	2.83	3.92[d]	2.78	2.18	4.46	2.96	5.40	6.70	3.48	4.48	4.89	5.89	6.99	3.64	4.40	4.46	4.47
Eu	0.87	–	1.06	1.01	1.39	0.97	1.50	1.25	1.06	1.17	1.30	1.49	1.23	1.01	1.05	1.07	1.21
Gd	2.84	–	3.17	2.71	4.84	2.88	5.80	7.21	3.53	4.51	4.91	6.06	6.89	3.96	4.36	4.75	4.81
Dy	2.65	–	3.15	2.66	4.86	2.97	5.62	8.11	3.52	4.39	4.80	5.87	6.94	3.69	4.43	4.62	4.96
Er	1.58	–	2.07	1.58	2.89	1.97	3.63	5.62	2.14	2.76	3.10	3.72	5.19	2.25	2.79	3.15	3.17
Yb	1.47	–	1.82	1.48	3.05	1.84	3.54	5.87	1.89	2.44	2.85	3.47	4.77	2.12	2.73	2.97	3.30
$^{87}Sr/^{86}Sr$	–	0.70340	0.70334	0.7032	0.70337	0.70324	0.70346	0.70331	0.70348	–	0.70339	0.70346	0.70344	0.70344	–	0.70333	0.70346
$^{143}Nd/^{144}$	–	0.513016	0.513025	0.513049	–	0.512994	–	0.512981	0.513001	–	0.513020	0.512989	0.512999	0.513027	–	0.513011	0.513000
Nd																	
$^{208}Pb/^{204}$	–	–	38.410	38.455	38.430	38.309	38.470	38.350	38.357	–	38.400	38.337	38.386	38.340	–	38.322	38.432
Pb																	
$^{207}Pb/^{204}$	–	–	15.578	15.615	15.584	15.555	15.597	15.551	15.557	–	15.582	15.548	15.566	15.551	–	15.550	15.580
Pb																	
$^{206}Pb/^{204}$	–	–	18.825	18.827	18.839	18.791	18.847	18.819	18.827	–	18.837	18.822	18.830	18.822	–	18.812	18.838
Pb																	

[a] SiO_2 and $^{87}Sr/^{86}Sr$ from Myers et al. (1986)
[b] SiO_2 and $^{87}Sr/^{86}Sr$ from Myers et al. (1985)
[c] Pb isotopic composition from Myers and Marsh (1987)
[d] Concentration determined by isotope dilution

Fig. 4. Plagioclase, olivine and clinopyroxene phenocryst compositions of a Nazan Bay basalt from the shield of Atka Volcano. Average plagioclase phenocryst compositions range from An_{69} to An_{86} (*left*). Coexisting groundmass plagioclase microlites are more albitic ($\leq An_{62}$). Olivine phenocrysts are relatively iron-rich (Fo_{63-70}) and unzoned (*right*). Coexisting clinopyroxene crystals are also rich in iron, of limited compositional range, and occur predominantly in glomerocrysts. *Open circles* Groundmass crystals, *closed circles* phenocrysts

Fig. 5. Average plagioclase phenocryst and microlite compositions of Korovin lavas. Phenocrysts range in average composition from An_{47} to An_{88}. In general, a single sample spans a large compositional range (>20 mol%) and the most sodic crystals overlap coexisting groundmass microlites. Rare, large, unzoned, calcic ($An_{\geq 90}$) xenocrysts occur in some samples. Based on core compositions, two phenocryst generations with different morphologies and zoning patterns are recognizable. Although one group has calcic cores and the other sodic ones, both generations have compositionally similar rims (*symbols* as in Fig. 4)

26 mol% An. In all Korovin samples, there is a significant overlap in composition between the most sodic phenocrysts and groundmass microlites (Fig. 5). The latter also display increasing compositional heterogeneity as bulk-rock silica increases. Many samples contain a few large, unzoned calcic (An_{90}) megacrysts. Similar crystals are common in other Aleutian lavas and have been interpreted as xenocrysts inherited from mafic liquid precursors (Brophy 1987; Singer et al. 1992a, 1992b; Myers 1993). Based on core compositions, plagioclase phenocrysts can be divided into calcic and sodic populations whose morphology and zoning vary (Linton et al.

1993). Phenocryst rims are compositionally similar to groundmass microlites.

Clinopyroxene compositions vary from $En_{38}Wo_{41}Fs_{15}$ to $En_{45}Wo_{35}Fs_{17}$ (Fig. 6). Within individual samples, clinopyroxene has a limited compositional range and individual crystals are weakly zoned (normal or reverse). The FeO^t/MgO ratios of phenocryst cores are near or less than those which would be in equilibrium with liquids having iron-magnesia ratios similar to the host rock (Linton 1993; Linton et al. 1993). Commonly, clinopyroxene crystals are rimmed by orthopyroxene and/or contain glass inclusions.

In the Korovin suite, olivine phenocrysts vary from Fo_{61} to Fo_{78}. Between samples, the variation in average olivine composition can be quite large. Crystals vary by just over 10 mol% Fo in the basalts whereas this range is nearly 20 mol% in the andesites (Fig. 6). Individual crystals are generally weakly (≤ 5 mol% Fo) normally zoned. The Mg#s of olivine cores do not correlate simply with bulk-rock FeO^t/MgO ratio, and individual samples are characterized by large variations in crystal core compositions, e.g., Mg# = 63–81 in AT-48. In the basalts, the Mg#s of the olivine cores are more Fe-rich than those which would have crystallized from liquids compositionally similar to the host bulk rock (Linton et al. 1993). In the andesites, by contrast, the crystal cores are too magnesia-rich relative to the bulk rocks.

Mount Kliuchef

Lavas from Mount Kliuchef contain from 0.4 to 4% clinopyroxene, 0–7.2% olivine, 21.6–36.4% plagioclase, and 0 to 0.6% oxides. Orthopyroxene (2.8%) replaces olivine as the low-Ca mafic phase in the most siliceous Mount Kliuchef lava (AT-88). In general, the percentage of phenocrysts decreases with increasing silica content. Relative to this suite, Korovin lavas have similar amounts of plagioclase, olivine and oxides but slightly more clinopyroxene. A lack of hydrous phases is, however, a characteristic shared by both suites.

Plagioclase phenocrysts in the basalts and basaltic andesites of Mount Kliuchef vary in size from just larger than the microlites to 1.6 mm in maximum dimension. In the most evolved lava, a dacite, some phenocrysts are much larger (≥3.5 mm). Plagioclase occurs as both isolated crystals and in glomerocrysts, are subhedral to euhedral and often broken. Plagioclase compositions are more calcic (An_{52} to An_{85}) in the basalts than in the more evolved dacites (An_{29} to An_{47}; Fig. 7). The most sodic phenocrysts are nearly 10 mol% more calcic than coexisting microlites, a characteristic which also distinguishes this suite from that of Korovin. Two generations of compositionally similar crystals with different zoning patterns can be identified. One population has unzoned cores surrounded by mantles and/or rims composed of euhedral, oscillatory zones (Linton et al. 1993). By contrast, complex-zoned and subrounded cores with glass inclusions characterize the other phenocryst generation. Normally zoned mantles and rims surround these cores.

Mount Kliuchef clinopyroxene phenocrysts occur mostly in glomerocrysts with plagioclase and olivine. Unlike the Korovin suite, the clinopyroxene crystals lack reaction rims and glass inclusions. They have average compositions of $En_{39–45}Wo_{34–42}Fs_{15–21}$, and within a single sample display limited compositional variability (Fig. 8). Zoning of individual crystals is relatively weak and can be either reverse or normal. Olivine phenocrysts range from Fo_{59} to Fo_{77}, a compositional span slightly larger than that of Korovin (Fig. 8). Compositional variability decreases with increasing bulk-rock silica content ($Fo_{59–78}$ vs. $Fo_{59–64}$). The compositional range within individual samples also decreases considerably from basalt (~20 mol%) to andesite (< 10 mol%). Both of these characteristics are unlike those of olivines in Korovin samples. Individual phenocrysts are weakly zoned (< 5 mol% Fo) and zoning is almost exclusively normal.

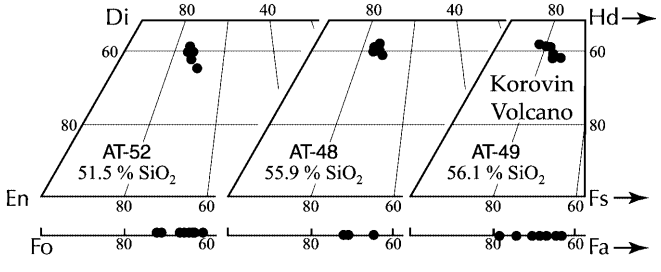

Fig. 6. Korovin olivine and clinopyroxene phenocryst compositions. Clinopyroxenes ($En_{38–45}Wo_{35–41}Fs_{15–17}$) are weakly zoned, occur almost exclusively in glomerocrysts and rimmed by orthopyroxene, and contain glass inclusions. Within individual samples, the range in compositions is limited. Coexisting olivines are smaller, mostly isolated crystals and relatively Fe-rich ($Fo_{\leq 78}$), even in the basalts. The compositional range of individual samples varies from 10 mol% in the basalts to almost 20 mol% Fo in the andesites (symbols as in Fig. 4)

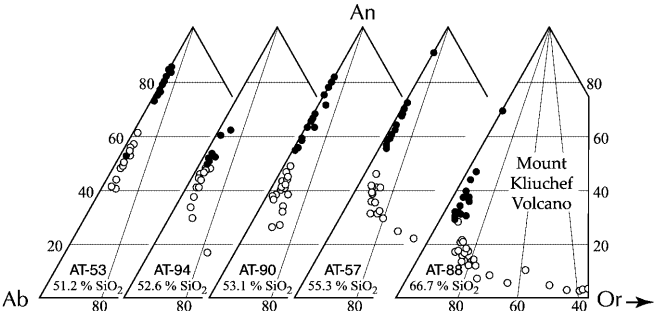

Fig. 7. Mount Kliuchef plagioclase phenocryst and microlite compositions. Plagioclase compositions are more calcic in the basalts than in the evolved dacites. Groundmass crystals in nearly all samples do not compositionally overlap coexisting phenocrysts but are at least 10 mol% more sodic (*symbols* as in Fig. 4)

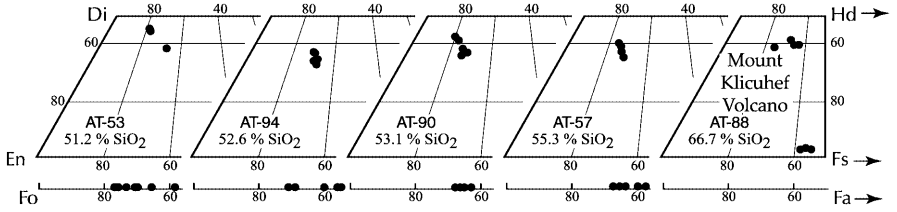

Fig. 8. Mount Kliuchef mafic phenocryst compositions. Clinopyroxene phenocrysts ($En_{39–45}Wo_{34–42}Fs_{15–21}$) are compositionally uniform within a single sample, occur mostly in glomerocrysts, and lack orthopyroxene rims and glass inclusions. These features distinguish them from clinopyroxenes in Korovin lavas. Individual crystals display weak zoning which may be either normal or reversed. Coexisting olivine phenocrysts range from Fo_{52} to Fo_{77} and increase in Fe/Mg ratio as bulk-rock silica increases. Unlike the clinopyroxene crystals, zoning is almost always normal but also weak (≤ 5 mol% Fo; symbols as in Fig. 4)

Geochemical results

Major elements

The three Atka volcanic suites, Atka Volcano, Korovin, and Mount Kliuchef, span the compositional range from basalt (48 wt% SiO_2) to dacite (66 wt% SiO_2), although the volumetrically dominant lavas are mafic (Table 4; Fig. 9). The suites are marked by relatively high alumina contents (16–21 wt%), CaO abundances between 10 and 5 wt%, and low magnesia (< 8 wt%). With increasing silica, Al_2O_3, FeO^t, MgO and CaO decrease but Na_2O and K_2O increase (Fig. 9). As for many Aleutian volcanic centers, TiO_2 forms a slightly convex trend. As noted by Myers et al. (1985), the Atka major-element trends are characterized by a high degree of coherency.

Although the three Atka volcanic suites fall along the same major-element compositional trends, their distribution along these trends are markedly different (Fig. 9). A continuous range in silica contents from basalt to dacite characterizes Atka Volcano, but the suite is dominated volumetrically by basalts (< 52 wt% SiO_2). The mafic and intermediate lavas define linear trends but the most siliceous unit, the Big Pink dacite, falls off these trends on the FeO^t and alumina plots. Neither the lavas of Mount Kliuchef nor those of Korovin show similar silica distributions (Fig. 9). Lavas of the former are marked by a distinct bimodal silica distribution. The majority of samples are basalts, basaltic andesites and andesites (< 55 wt% SiO_2) whereas two samples are dacites with silica contents of 66 wt%. No lavas occur between these two groups. The Korovin suite differs from those of both Atka Volcano and Mount Kliuchef. It varies from 51.5 to 62.5% silica, with intermediate lavas clustering around 55% SiO_2. For nearly all major-element oxides, these andesites lie along linear trends between the mafic and siliceous lavas (Fig. 9). The Korovin dacite is slightly less siliceous than similar units from the other two volcanic vents.

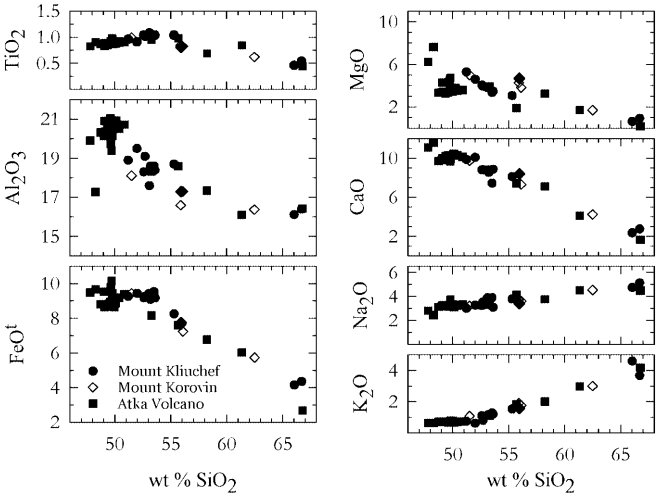

Fig. 9. Major-element Harker diagrams for the Atka volcanic suite. The lavas from this volcanic center span the compositional range from basalt to dacite. With increasing silica, Al_2O_3, FeO^t, MgO and CaO decrease systematically whereas Na_2O and K_2O increase. TiO_2 displays a convex pattern with a maximum near 55 wt% SiO_2. Lavas from Atka Volcano, Korovin and Mount Kliuchef fall along the same major-element trends but their distributions along these trends are different. Atka varies continuously from basalt to dacite but is dominated by mafic lavas. All except two Mount Kliuchef lavas have silica contents of less than 55 wt% SiO_2. The most siliceous lavas of both Mount Kliuchef and Atka Volcano have 66 wt% SiO_2. Korovin lavas form three groups. The mafic basalts are similar to those of the other two vents. By contrast, the most evolved Korovin lavas contain less silica (62 wt%) than the other dacites. The third Korovin compositional group consists of andesites which plot intermediate between the mafic and siliceous lavas. *Closed squares* Atka Volcano, *closed circles* Mount Kliuchef, *open diamonds* Korovin Volcano, *closed diamond* Kay and Kay (1994) sample from NE of Korovin summit

Trace elements

On many trace-element Harker diagrams, the Atka suite defines linear trends (Table 4; Fig. 10). With increasing silica, Rb, Y, Zr and Ba increase whereas Sr and V decrease. However, Ni and Cr display more complex patterns. At silica contents greater than about 53 wt%, the abundances of these compatible elements are low (≤ 30 ppm for Ni and ≤ 50 ppm for Cr). By contrast, the ranges for these elements in Atka basalts are quite large (Fig. 10).

When considered by individual volcanic vent, differences in the trace-element trends distinguish Korovin from Mount Kliuchef and Atka Volcano. The Korovin samples are compositionally uniform, e.g., 437–481 ppm Sr, 24–31 ppm Y, 90–146 ppm Zr, 429–565 ppm Ba, 44–

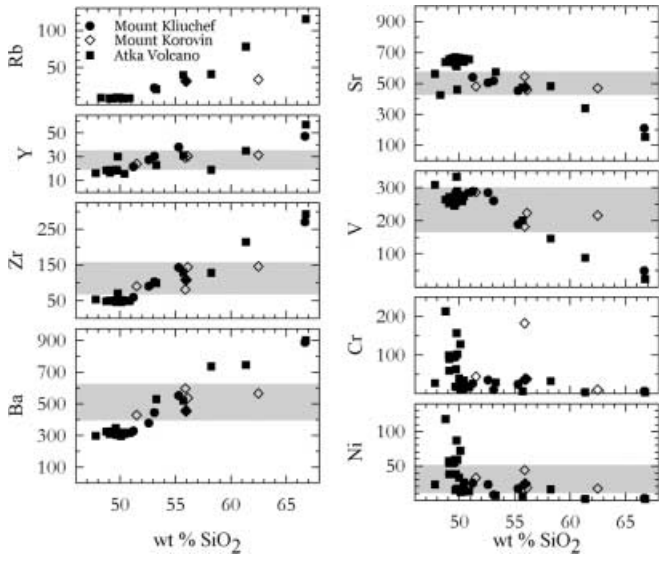

Fig. 10. Trace element abundances plotted against silica for Atka lavas. With increasing SiO_2, Rb, Y, Zr, and Ba increase but Sr decreases slightly and V substantially in the lavas from Atka Volcano and Mount Kliuchef. The Korovin samples do not show significant variations in trace element abundances but define horizontal bands (*shaded bands*) when plotted against silica. With one exception, Cr and Ni abundances are low throughout the Korovin and Mount Kliuchef suites. By contrast, mafic lavas from Atka Volcano (< 52 wt% SiO_2) display a large range in compatible element contents (Cr < 213 ppm; Ni < 118 ppm; *symbols* as in Fig. 9)

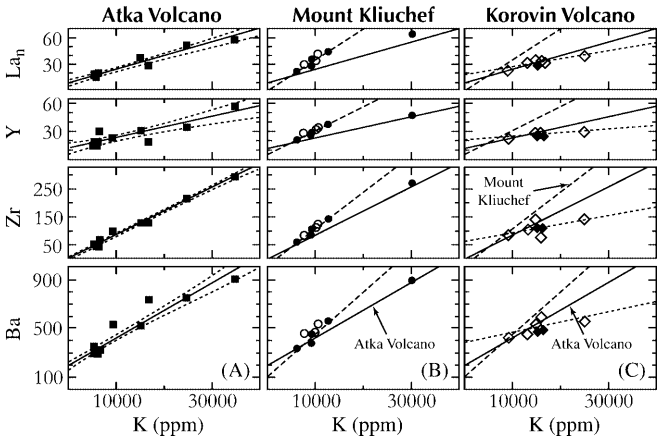

Fig. 11a–c. Incompatible elements plotted against K for the three Atka volcanic suites. **a** For all four elements, Atka Volcano lavas define linear trends which do not pass through the origins (*dotted lines* represent 2 σ errors for the linear regression). Two samples from a geographically restricted region of the volcano plot above the general Ba–K trend. **b** Mount Kliuchef basalts through andesites (*closed circles*) define linear trends (*dashed lines*) with steeper slopes than the corresponding trends for Atka volcano (*closed lines*). For all elements, the Kliuchef dacite (denoted by the *closed circle* with 30,000 ppm K) falls below the mafic lava trends and on those for Atka Volcano. Trace-element abundances calculated for the mafic lavas using fractionating solid proportions based on major elements and Rayleigh fractionation (*open circles*) reproduce the observed abundances well for all elements (see text for modeling details). The Mount Kliuchef dacite cannot be related to the andesites by fractionation of the observed phenocryst assemblage. The liquid parental to this lava may represent a crustal partial melt or, because it lies on the Atka Volcano trends, it may be a liquid tapped from the earlier magmatic phase. In either case, the lack of lavas intermediate between the andesites and dacite suggests that significant mixing with more mafic liquids did not occur. **c** The Korovin Volcano suite (*open diamonds*) falls along shallow linear trends which are markedly different from those of the other two suites. The significant displacement of these trends from the origin suggests they are mixing lines between basalt and dacite. Trace-element abundances calculated from end-member proportions estimated from major-element mass balance modeling (*closed diamonds*) reproduce observed abundances well for $(La)_n$ and Y, and moderately well for Zr and Ba. Because it lies off the Atka Volcano and Mount Kliuchef trends, the Korovin dacite is unlikely to be related to either of these other volcanic systems. It probably represents a crustal partial melt

182 ppm Cr, and 18–44 ppm Ni, and define broad horizontal bands on Harker diagrams (Fig. 10). Although part of these more limited compositional ranges may be due to the slightly less evolved nature of the Korovin dacites, they are depleted in incompatible elements compared to Atka Volcano and Mount Kliuchef lavas of similar silica contents (Table 4). For Cr and Ni, one sample from Korovin plots considerably above the trend for the rest of the suite and differs in trace-element abundances from other samples of similar silica levels (Fig. 10).

On incompatible element-K plots, the three Atka volcanic suites behave differently. For Atka Volcano, all samples fall along linear trends (Fig. 11a). Except for Zr, the linear trends do not pass through the origin. Two geographically related samples plot above the general trend on the Ba–K plot. By contrast, not all of the Mount Kliuchef samples fall along common trends. The mafic samples (< 56% SiO_2) define linear trends with slopes greater than those of Atka Volcano which pass close to the origins for most elements. The Kliuchef dacites fall considerably below the mafic lava trends and plot on those for Atka Volcano (Fig. 11b). The Korovin Volcano suite defines linear trends with shallower slopes than either Atka Volcano or Mount Kliuchef (Fig. 11c). These trends have large incompatible element intercepts. Similar relationships are evident when incompatible elements are plotted against Rb instead of K.

Rare earth elements

The Atka lavas are slightly LREE-enriched ($(La/Yb)_n = 2.13–3.52$), with both positive and negative Eu anomalies ($Eu/Eu^* = 1.28–0.54$; Table 5). As with the trace elements, significant differences distinguish the rare earth element characteristics of the three Atka suites. For all samples, Atka Volcano REE abundances increase systematically with increasing silica content (Fig. 12a). For example, $(La)_n$ changes progressively from 14.71 to 58.82 over a silica range of 47.8 to 66.8 wt%. One andesite (AT-34) with a $(La/Yb)_n$ ratio higher than other Atka Volcano samples overlaps the basalts in HREEs. This sample is also one of the samples which lies above the Ba–K trend. With increasing silica,

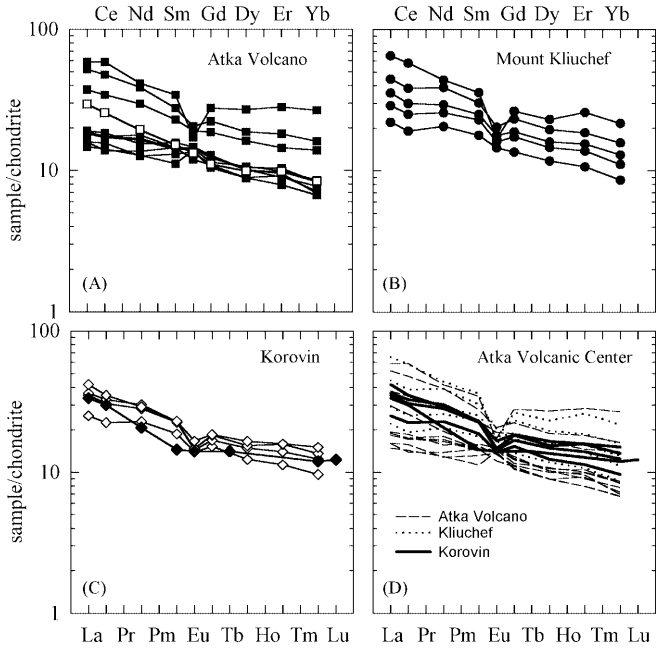

Fig. 12a–d. Chondrite-normalized rare-earth element patterns for the Atka volcanic complex. Unlike the major elements, significant differences characterize the REE patterns of the three different Atka vents. **a** With increasing silica, REE abundances of Atka Volcano lavas increase systematically and Eu anomalies become more negative. One sample (AT-34, *open square*) has an unusually high $(La/Yb)_n$ ratio of 3.52. This sample also falls off the Atka Volcano Ba–K trend (Fig. 11a). **b** Like Atka Volcano samples, Mount Kliuchef samples have REE abundances which increase systematically with SiO_2. No REE patterns crosscut each other. **c** In contrast to Atka Volcano and Mount Kliuchef samples, there is no systematic correlation between REE abundances and SiO_2 for the Korovin lavas. Instead, the patterns overlap. The sample (*closed diamond*) analyzed by Kay and Kay (1994) has a REE pattern which cuts steeply across those determined in this study. **d** Comparison of the REE characteristics of the three Atka volcanic vents. Korovin lavas fall in the middle of the range for the other two suites, despite spanning only a slightly narrower silica range. Note the similarity in pattern and Eu/Eu* between the Atka Volcano and Kliuchef dacites (normalizing chondrite values from Wakita et al. 1971)

Eu anomalies become more negative (Fig. 12a). For the suite, Eu/Eu* decreases from 1.28 in the basalts to 0.55 in a dacite. Like the Atka Volcano lavas, REE abundances in Mount Kliuchef samples increase systematically with silica (Fig. 12b). Over a silica range from 51.2 to 66.7 wt%, $(La)_n$ varies from 22.09 to 65.29. Relative to Atka Volcano, a slightly smaller Eu/Eu* range (0.92–0.54) is evident in the Mount Kliuchef suite. The Kliuchef dacite has a REE pattern and Eu/Eu* anomaly very similar to those of the Big Pink dacite of Atka Volcano. In contrast to these two suites, Korovin lavas display only a small increase in REE abundance (e.g., $(La)_n = 25.12–41.76$) over a slightly narrower silica range, i.e., 51.5 to 62.5 wt%. Consequently, individual samples plot on top of each other on the chondrite-normalized diagram (Fig. 12c). Eu anomalies are negative (0.71–0.82) but nearly constant throughout the suite. Korovin $(La/Yb)_n$ ratios vary from 2.61 to 2.82, a slightly narrower range than those for the other two volcanic vents (Atka Volcano: 2.13–3.52; Mount Kliuchef: 2.57–3.01). The sample analyzed by Kay and Kay (1994) has a REE pattern which cuts across those of the other Korovin samples (Fig. 12c).

On process-identification diagrams, i.e., $(La/Yb)_n$ vs. $(La)_n$ and $(La/Sm)_n$ vs. $(La)_n$, all three Atka suites fall along the same horizontal trends (Fig. 13). For Mount Kliuchef and Atka Volcano lavas, the samples are arranged along this trend, with the most mafic lavas on the left and the more evolved to the right. On both of these diagrams, the distinctive lavas for Atka Volcano and Kliuchef are not distinguishable from the other samples from those centers.

Sr, Nd and Pb isotopes

Six new, initial Sr isotopic analyses are characterized by limited variability, i.e., $^{87}Sr/^{86}Sr = 0.70333–0.70348$ (Table 5). Previously reported Sr isotopic ratios range from $^{87}Sr/^{86}Sr = 0.70318$ to 0.70345 (Myers et al. 1985, 1986), thereby defining a slightly greater degree of isotopic variability. Because the new analyses are confined to Mount Kliuchef and Korovin samples, these suites are marked by less variability than Atka Volcano which is represented by older analyses. Although the greater homogeneity of Mount Kliuchef and Korovin may be related to the smaller number of analyses, it probably reflects an increase in the precision of strontium isotopic

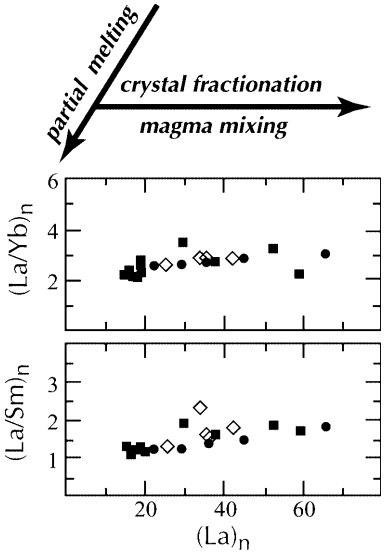

Fig. 13. $(La/Yb)_n$ and $(La/Sm)_n$ versus $(La)_n$ process-identification diagrams. On both sets of diagrams, the Atka suite defines narrow horizontal trends with considerable overlap between the three suites. In contrast to Atka Volcano and Mount Kliuchef lavas, Korovin samples cover only a limited portion of the trends. Horizontal trends such as those shown here are consistent with formation of the suites by crystal fractionation or mixing of end-member magmas located at either end of the trends (symbols as in Fig. 9)

analysis. Nd isotopic compositions vary from $^{143}Nd/^{144}Nd = 0.512981$ to 0.513049 (Table 5). When plotted against silica, the Atka suite forms a horizontal band (Fig. 14). Lead isotopic ratios range from 38.322 to 38.432 for $^{208}Pb/^{204}Pb$, and 15.548 to 15.580 for $^{207}Pb/^{204}Pb$, with $^{206}Pb/^{204}Pb$ between 18.766 and 18.860 (Table 5). These values are within analytical error of those previously reported by Myers and Marsh (1987). As with the other isotopic systems, there is no significant variation in isotopic composition with silica (Fig. 14). For all isotopic systems, the lavas with unusual trace- and rare-earth element contents cannot be distinguished from the rest of the Atka suite.

Discussion

The three Atka volcanic suites, i.e., Atka Volcano, Mount Kliuchef and Korovin, share the following common characteristics: (1) an anhydrous phenocryst assemblage of plagioclase ± olivine, clinopyroxene and a single Fe–Ti oxide; (2) similar major-element compositions; (3) overlapping compositional trends on rare-earth element process-identification diagrams; and (4) identical Sr, Nd and Pb isotopic characteristics. The major-element compositional similarity of the mafic lavas suggests each vent was supplied by similar parental magmas. In addition, their isotopic homogeneity indicates that contamination (lithospheric or crustal) did not occur, was minor or involved materials isotopically similar to the parental magmas. Because of systematic and coherent trace- (Figs. 10 and 11) and rare-earth (Figs. 12 and 13) element trends, significant contamination probably did not occur. Assimilation of large amounts of crustal material, even of similar isotopic composition, probably would have produced more complex trace- and RE element characteristics than those observed. A lack of contamination is also suggested by comparison with other Aleutian centers. In particular, Singer et al. (1992a, 1992b) showed that at Seguam systematic and coherent compositional trends and isotopic homogeneity were indicative of closed-system crystal fractionation with little contamination. By contrast, open-system processes involving significant magma wall rock interaction were suggested by the compositional variability of Adak rocks (Myers et al. 1985; Myers and Frost 1994).

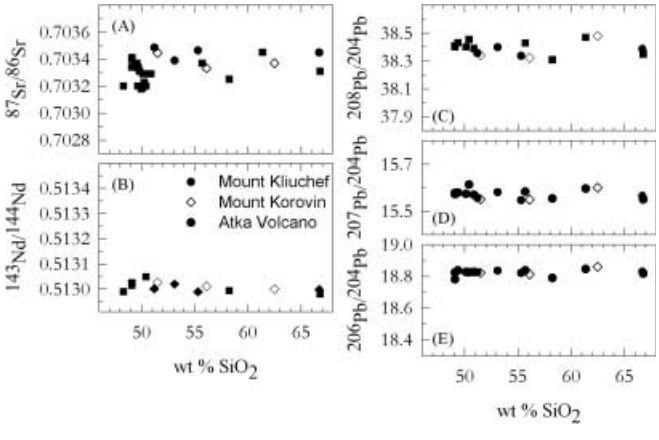

Fig. 14. Initial Atka strontium, neodymium and lead isotopic ratios plotted against silica. The volcanic suite defines narrow horizontal bands for all three isotopic systems, with complete overlap between the three intracenter volcanic suites. Individual error bars are shown for previously published Sr isotopic data. Analytical errors for the new isotopic results are shown by *crosses* in the lower left corners of the diagrams (data from this study, and Myers et al. 1985, 1986; *symbols* as in Fig. 9)

Despite their common features, the Atka intracenter volcanic suites are distinguished by significant differences. For example, Korovin differs from Atka Volcano and Mount Kliuchef in (1) plagioclase phenocryst compositions and zoning patterns; (2) clinopyroxene-groundmass relations; (3) silica distributions; (4) trace-element abundances; (5) incompatible vs. incompatible element trends; (6) correlation between REE abundance and SiO_2 content; and (7) the nature and magnitude of Eu anomalies. All three volcanic suites have different incompatible-incompatible element trends and rare-earth element features. These differences suggest the same magmatic processes did not produce all three suites or that the same process worked differently at the three vents.

Atka Volcano

The systematic major- and trace-element vs. SiO_2 trends (Figs. 9 and 10), linear incompatible-incompatible element trends (Fig. 11a), increase in REE abundance with silica, positive correlation between SiO_2 and Eu/Eu* (Fig. 12), horizontal trends on the REE process-identification diagrams (Fig. 13), and limited isotopic variability (Fig. 14) all suggest that crystal fractionation and/or magma mixing may have played an important role in generating the Atka Volcano suite. A magma mixing origin for this suite requires a siliceous end member to interact with the basaltic magma which produced the basal shield of Atka Volcano. No evidence of an independent siliceous end member is preserved on Atka. Therefore, a crystal fractionation origin of the suite is preferred.

Mount Kliuchef

To evaluate a crystal fractionation origin for the Mount Kliuchef suite, quantitative tests of potential fractionation paths were performed using least-squares mass balance procedures. Two different fractionation schemes were tested (Table 6). Model 1 assumed the suite was generated by progressive fractionation, i.e., fractionation of an observed phenocryst assemblage produced an evolved liquid represented compositionally by the next most siliceous lava. Because plagioclase phenocrysts in

Table 6. Crystal fractionation models

Volcano	Mount Kliuchef: model 1				Mount Kliuchef: model 2			Korovin Volcano		
Sample #	AT-53, AT-94, AT-90, AT-57, AT-88				AT-53, AT-90, AT-57, AT-88			AT-52, AT-48, AT-49, AT-117		
SiO_2	51.40 ⇒ 52.6 ⇒ 53.41 ⇒ 55.05 ⇒ 66.13				51.40 ⇒ 53.41 ⇒ 55.05 ⇒ 66.13			51.81 ⇒ 52.16 ⇒ 57.06 ⇒ 63.11		
Stage	1a	1b	2	3	1	2	3	1	2	3
Plag	17.3	14.3	6.1	81.0	25.2	6.1	81.0	30.4	1.1	38.1
Ol	6.6	2.6	0.8	5.1	8.9	0.8	5.1	13.4	0.3	12.3
Cpx	4.1	1.4	6.9	24.2	4.0	6.9	24.2	1.5	7.1	8.5
Tmt	–	0.4	2.3	11.1	–	2.3	11.1	–	–	–
Σr^2	0.14	0.64	0.33	1.27	0.22	0.33	1.27	7.98	0.40	4.75
F (%)	72.0	81.2	83.9	–21.5	62.0	83.9	–21.5	57.7	92.1	41.1
F parent (%)	72.0	58.3	48.9		62.0	52.0		57.7	53.1	21.8

AT-94 are more sodic than those of the other basalts and basaltic andesites (Fig. 7), an alternative scheme (model 2) involving fractionation directly from basalt (AT-53) to basaltic andesite (AT-90) was also tested. For both schemes, the sum of the square of the residuals for the different fractionation stages range from 0.144 to 0.644 (Table 6), suggesting the various parents and daughters could be related by the proposed fractionation schemes. The highest residual (0.644) involves fractionation from AT-94, the sample with the anomalous plagioclase phenocrysts, to AT-90. For all stages, the solid assemblage removed is dominated by plagioclase (6–25%), with lesser amounts of olivine (< 9%), clinopyroxene (1.4–6.9%) and Fe–Ti oxide (< 3%). Calculated fractionating solid percentages, i.e., decreasing olivine and increasing cpx with increasing silica, mimic observed phenocryst abundances (i.e., decreasing olivine as cpx increases from basalt to andesite). Generation of the basalt to andesite Mount Kliuchef lavas by fractionation would require fractionation of between 48 and 52% of the original basaltic parental magma (Table 6).

Using the calculated solid proportions and assuming Rayleigh fractionation, trace- and rare-earth element contents were calculated for each fractionation stage. To maintain consistency with previous Aleutian studies, the distribution coefficients used by Singer et al. (1992a) were employed. In general, observed trace-element abundances agree well with calculated values. For most trace elements, calculated and observed abundances are within 20–25% of each other. The greatest discrepancy is for Cr, for which calculated values are always lower than observed values. On incompatible-incompatible element diagrams, the calculated concentrations fall along the linear trends defined by the mafic lavas (Fig. 11a). The REE patterns calculated for each fractionation stage also mimic observed patterns (Fig. 15a). Agreement is best for the mafic lavas but decreases in the andesitic range. In particular, the REE pattern of the calculated andesite is lower on the chondrite-normalized diagram, with a slightly higher $(La/Yb)_n$ ratio. In light of the observed variation in K_D values, the agreement between observed and calculated trace- and RE element abundances is compatible with a crystal fractionation origin for the mafic Mount Kliuchef lavas.

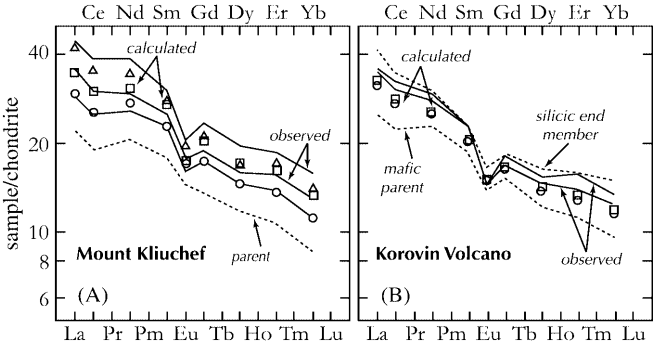

Fig. 15a, b. Comparison of calculated and observed rare-earth element patterns for Mount Kliuchef and Korovin Volcano. **a** Calculated REE abundances (*open symbols*) for the basalts through andesites of Mount Kliuchef are, in general, in good agreement with the observed patterns (*closed lines*). Agreement is best for the basalts and andesitic basalts, with both overall abundances and slope agreeing well. The REE pattern of the parent is shown by the *dotted line*. **b** Mixing of the Korovin basalt and dacite (*dashed lines*) produces REE patterns of variable match to the observed andesites. For AT-49, the fit is good, particularly for the heavy REE. By contrast, the calculated abundances fall consistently below the observed pattern for AT-48

As suggested by the incompatible elements, the dacite could not have been produced from the andesite by crystal fractionation (Table 6). Mass balance models yield unrealistic solid assemblages, a negative liquid fraction and very high residuals. Noting the compositional similarity between the dacites of Mount Kliuchef and Atka Volcano and the position of the former on the incompatible element trends for Atka Volcano (Fig. 11b), at least three alternative origins can be suggested for the Mount Kliuchef dacite. It may represent (1) a crustal melt, (2) a complete melt of solidified Big Pink magma, or (3) an independent magma tapped from the earlier Atka Volcano plumbing system. Regardless of its origin, this dacitic liquid must have interacted little with the more mafic magmas in the Mount Kliuchef crustal plumbing system.

Korovin Volcano

In contrast to Atka Volcano and Mount Kliuchef, many of the features of the Korovin lavas are suggestive of open-system processes. These characteristics include multiple plagioclase phenocryst generations, orthopyroxene overgrowths on clinopyroxene, glass inclusions in clinopyroxene, the lack of correlation between Eu/Eu* and bulk-rock silica, and the limited ranges in incompatible trace-element abundances. Unlike Atka Volcano and Mount Kliuchef, several geochemical characteristics of the Korovin suite suggest that these lavas were not produced by crystal fractionation. In particular, the absence of an increase in REE abundances with increasing silica, and the tight clustering of the Korovin samples on the REE process identification diagrams are all inconsistent with an origin by crystal fractionation. This conclusion is supported by mass balance results (Table 6) which produced large residuals for all but one of the likely fractionation steps (Table 6).

Because they lie along a linear trend between basalt and dacite, the andesites of Korovin Volcano may have been produced by magma mixing. Such a process would be consistent with the observed petrographic characteristics. Assuming the Korovin andesites were produced by mixing basaltic parent (AT-52) with the most siliceous lava (AT-117), mixing models were performed for the two Korovin andesites (Table 7). The quality of the fit for the two andesites varies considerably. For AT-49, the sum of the square of the residuals is 0.44, suggesting a relatively good fit. This result is not surprising because AT-49 lies close to the mixing lines for the majority of incompatible element systems (Fig. 11c). Differences between calculated and observed trace- and rare-earth element abundances are also small (Table 7). Calculated chondrite-normalized REE patterns mimic the observed pattern for AT-49 very well, especially for the heavy REEs (Fig. 15b). Production of AT-49 by magma mixing would require a nearly 50:50 mix of the two end members (Table 7). By contrast, mixing produces a much worse match for AT-48, e.g., $\Sigma r^2 = 1.76$. In addition, the differences between calculated and observed trace- and rare-earth element abundances are consistently higher in this case than for AT-49. Calculated REE abundances consistently fall below the observed values (Fig. 15b). The mismatch for this sample could reflect processes such as fractionation which occurred after mixing, thereby shifting the liquid composition away from the mixing line.

Table 7. Magma mixing models for Korovin Volcano andesites

	0.62(AT-52) + 0.38(AT-117) = AT-48			0.55(AT-52) + 0.45(AT-117) = AT-49		
	Observed	Calculated	Δ	Observed	Calculated	Δ
SiO_2	56.16	55.96	0.20	57.06	57.03	0.03
TiO_2	0.84	0.86	0.02	0.83	0.84	0.01
Al_2O_3	16.68	17.55	0.87	17.60	17.51	0.09
FeO^t	7.66	8.10	0.44	7.37	7.88	0.51
MnO	0.14	0.14	0.00	0.18	0.14	0.04
MgO	4.29	3.78	0.51	3.89	3.56	0.33
CaO	8.41	7.71	0.70	7.42	7.35	0.07
Na_2O	3.73	3.73	0.00	3.66	3.84	0.18
K_2O	1.91	1.82	0.09	1.80	1.96	0.16
P_2O_5	0.18	0.21	0.03	0.18	0.21	0.03
Σr^2			1.76			0.44
Sr	544	476	68	457	477	20
Y	29	27	2	30	27	3
Zr	81	111	30	144	115	29
Ba	597	479	118	537	491	46
Sc	26	29	3	27	29	2
V	182	259	77	223	255	32
Cr	182	31	151	38	29	9
Ni	44	27	17	18	26	8
La_n	35.00	31.31	3.69	36.18	32.65	3.53
Ce_n	30.66	27.11	3.55	32.64	28.15	4.49
Nd_n	28.13	25.11	3.02	30.16	25.68	4.48
Sm_n	22.56	20.23	2.33	22.87	20.63	2.24
Eu_n	14.38	14.84	0.46	14.66	15.11	0.45
Gd_n	16.77	16.43	0.34	18.27	16.74	1.53
Dy_n	14.77	13.86	0.91	15.40	14.23	1.17
Er_n	13.95	12.95	1.00	15.75	13.35	2.40
Yb_n	12.41	11.63	0.78	13.50	12.07	1.43
$(La/Yb)_n$	2.78	2.69	0.09	2.78	2.70	0.08
$(La/Sm)_n$	1.82	1.55	0.27	1.82	1.58	0.24
$(Ce/Yb)_n$	2.34	2.33	0.01	2.34	2.33	0.01
$(Ce/Sm)_n$	1.53	1.34	0.19	1.53	1.36	0.17
$(Eu^*/Eu)_n$	0.80	0.81	0.01	0.80	0.81	0.01

Crustal magmatic system

The evolution of the Atka volcanic center began with the formation of Atka Volcano. Early eruptions of numerous, thin flows from a large number of spatially isolated volcanic vents produced a large basal shield (Fig. 16a). These lavas were high-alumina basalts of relatively uniform composition. The limited compositional variability of the high-alumina basalts probably reflects small degrees of crystal fractionation. Although the compositional similarity of these flows suggest their vents were supplied from one large, communicating magma chamber, they may also have erupted from a series of small, isolated chambers fed with the same parental basaltic magma. As the system evolved, active volcanic vents became concentrated in the center of the basal shield. Eruptions from these vents subsequently produced Atka Volcano proper and the subsidiary vents located around the flanks of this larger stratocone (Fig. 16b). At the same time, compositions of erupted lavas shifted from basalt to basaltic andesite through andesite. The quantitative modeling and the linear incompatible-incompatible element trends suggest this change in composition reflects crystal fractionation of the high-alumina basaltic magma. Physically, the shift in vent distribution and composition can be interpreted in two ways: (1) decrease in the volume of a single magma chamber; or (2) a declining magma supply rate resulted in the abandonment of the peripheral chambers. Either scenario could result from a cooling magmatic system undergoing increased crystallization and fractionation. The final stage in the development of the Atka Volcano plumbing system is edifice collapse producing the Atka caldera and eruption of the Big Pink dacite (Fig. 16c). As with the intermediate lavas, the Big Pink dacite was also derived by crystal fractionation. The extremely large volume of the Atka Volcano basal shield and associated cones suggests that its growth and evolution must have significantly perturbed the crust thermally. Subsequent volcanism occurred in a region preheated by

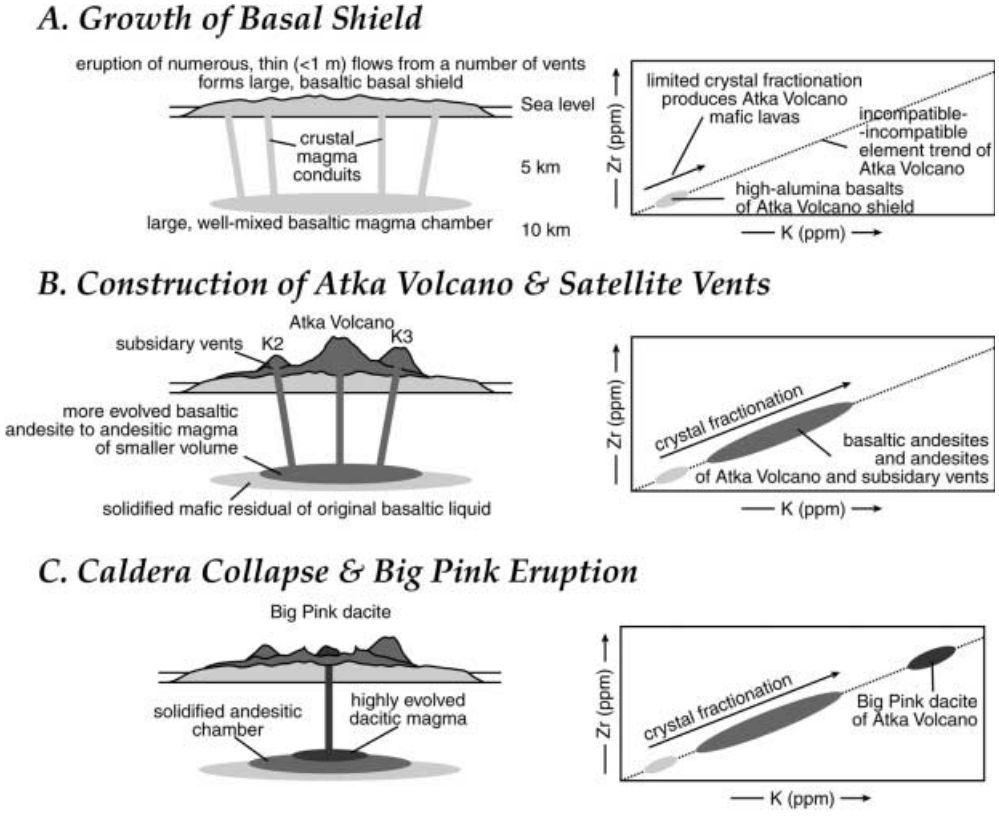

Fig. 16a–c. Schematic diagram depicting the development of the magmatic system which supplied Atka Volcano. **a** The basal shield of Atka Volcano was formed by eruption of numerous thin flows from a large number of spatially isolated vents (*left*). These vents could have been supplied from one large, communicating magma chamber as shown, or by a series of small but isolated systems. The Atka basalts are marked by a limited range in composition. This limited variability could result from small degrees of crystal fractionation, as shown on the Zr vs. K diagram (*right*). **b** As the system cooled and/or the magma supply rate declined, the volume of the magma chamber decreased or the peripheral chambers were abandoned and solidified. Eruption of these lavas from this spatially restricted plumbing system produced Atka Volcano proper and the subsidiary vents located around the flanks of this larger stratocone (*left*). The Zr–K linear trend of the basaltic andesites and andesites suggests that they were formed by crystal fractionation (*right*). At the same time, the extension of this trend through the Atka Volcano basalt field suggests these basalts were probably parental to the more evolved liquids. **c** Collapse of Atka Volcano produced the Atka caldera. The Big Pink dacite was subsequently erupted on the caldera floor (*left*). This unit represents the last stage of the Atka Volcano plumbing system. The positioning of this unit on the Zr–K diagram is also consistent with its derivation by closed-system crystal fractionation from the andesites (*right*)

earlier magmatism. This heating may have played an important role in determining the manner in which the later Kliuchef and Korovin crustal systems evolved.

The Mount Kliuchef volcano was constructed by the eruption of a series of basalt through andesite lava flows (Fig. 17a). As for Atka Volcano, these lavas were produced by closed-system fractionation of a solid assemblage of pl + ol + cpx ± tmt from a parental high-alumina basalt. Because this assemblage does not occur at less than 10 kbar under anhydrous conditions (Baker and Eggler 1987), these chambers must have resided at depths greater than 9 km if the magmas were dry. The presence of the water in the system could change the place of the magma chambers in the depth range of 3 to 8 kbar (Eggler 1972; Eggler and Burnham 1973; Sekine et al. 1979). The different incompatible-incompatible element slopes between the Atka Volcano and Kliuchef suites require that there is some difference in the process between the two suites. As discussed above, this difference could be slight differences in parent trace-element composition or the degree of trace-element incompatibility. Because it does not lie on the Zr–K trend defined by the more mafic lavas, the Mount Kliuchef dacite cannot be related to the latter by crystal fractionation (Fig. 17b). The dacite may represent a crustal partial melt or residual magma tapped from the earlier Atka Volcano plumbing system. The absence of lavas intermediate between the andesites and dacites of Mount Kliuchef suggests little mixing occurred between these two liquids.

Although the Korovin suite also ranges from basalt to dacite and forms linear incompatible-incompatible element trends, these trends differ in slope from those of both Atka Volcano and Mount Kliuchef. Because it is compositionally unlike any of the other evolved lavas of the Atka suite, the siliceous end member, a dacite, must have been produced by a petrologic process completely different from that forming the other evolved liquids. Consequently, we suggest it was formed by crustal fusion (Fig. 18a). The linear trend for the entire suite as well as its petrographic characteristics suggest an origin by magma mixing (Fig. 18b). For both of the younger Atka volcanic systems, the thermal perturbation of the arc crust earlier by the much larger Atka Volcano system had profound implications for the development of the Korovin and Kliuchef suites. The crustal heating permitted the later but smaller volume systems to evolve through crystal fractionation (Mount Kliuchef) and to produce small amounts of crustal melting (Korovin).

Fig. 17a, b. Development of the Mount Kliuchef magma plumbing systems. **a** The Mount Kliuchef volcano was constructed by the eruption of a series of basalt through andesite lava flows (*left*). These lavas were produced by closed-system fractionation of a solid assemblage of pl + ol + cpx ± tmt from a parental high-alumina basalt similar to that of Atka Volcano. Because they lie along a Zr–K linear trend which differs from that of Atka Volcano, the Mount Kliuchef lavas could not have been produced by a similar fractionation process (*right*). **b** The Mount Kliuchef dacite does not lie on the Zr–K trend defined by the more mafic lavas (*right*). Consequently, it cannot be related to the andesites by crystal fractionation. The dacite may represent a crustal partial melt or residual magma tapped from the earlier Atka Volcano plumbing system (*left*). The absence of intermediate lavas between the andesites and dacites of Mount Kliuchef suggests little mixing occurred between these two liquids (see text for detailed discussion)

Conclusions

Quaternary volcanic activity at the Atka volcanic center produced (1) a shield volcano, Atka Volcano, dominated by basalt and basaltic andesite; (2) its satellite vents; (3) a caldera and associated dacitic flow; and (4) four major volcanoes around the caldera margin – Korovin, Mount Kliuchef, Sarichef and Konia. The lavas from these volcanic vents have an anhydrous phenocryst assemblage, similar major-element compositional ranges (basalt to dacite), and nearly identical Sr, Nd and Pb isotopic ratios. However, there are significant differences in lavas from different vents. Petrographic differences

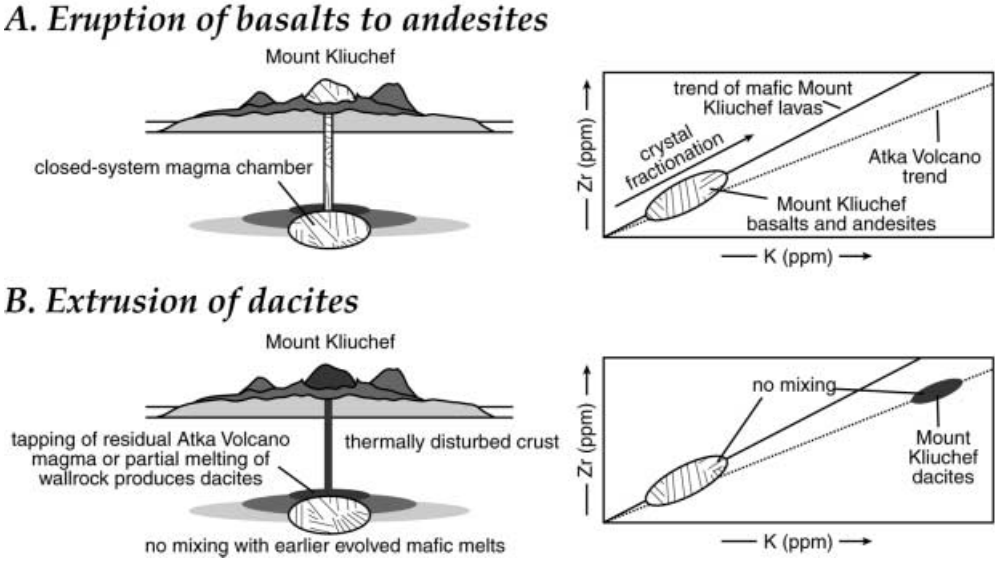

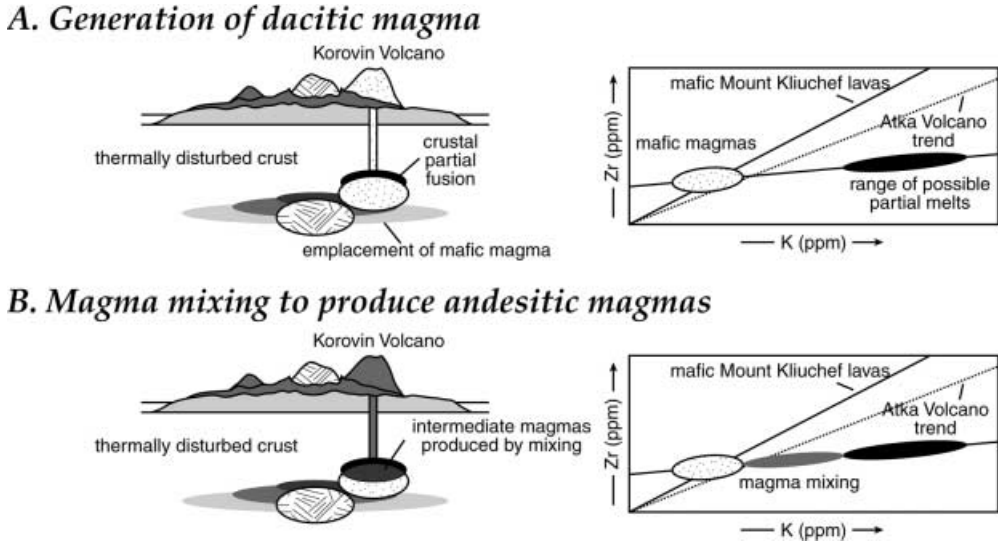

Fig. 18a, b. Evolution of the Korovin magmatic plumbing system. **a** Intrusion of basaltic magma into the warm crust initiated a small amount of crustal partial melting (*left*). The thermal perturbation of the crust by the much larger Atka Volcano system permitted the relatively minor amount of basaltic magma associated with the Korovin system to melt its crustal wall rock. This partial melt did not lie along the Zr–K trends characteristic of either Atka Volcano or Mount Kliuchef (*right*). **b** Mixing of the crustal partial melt and the parental basaltic magma produced the intermediate andesites erupted from Korovin (*left*). Thus, these lavas line along a linear Zr–K trend unlike those of other Atka volcanic centers (*right*; see text for additional discussion)

include variations in plagioclase compositions and zoning patterns, and the absence or presence of clinopyroxene phenocrysts. Lavas from each vent are also marked by trace- and rare-earth element differences.

Petrographic, geochemical and isotopic characteristics of the Atka volcanic center suggest that the basaltic to dacitic suite of Atka Volcano formed by crystal fractionation of an anhydrous phenocryst assemblage. Mount Kliuchef mafic lavas likewise were produced by crystal fractionation, but the Mount Kliuchef dacites represent crustal melts or residual liquids from the Atka Volcano magmatic system. The Korovin basalt to dacitic suite formed in a different manner. The evolved lavas from this center formed by partial melting. Mixing of this magma with the parental basaltic magma produced the intermediate andesite.

The Atka data suggest (1) large volcanic centers may be supplied by a series of non-communicating, crustal magma chambers; (2) local factors may be important in determining liquid-lines-of-descent; and (3) very different magmatic processes may occur in adjacent magma chambers.

Acknowledgements Analytical work for this project was supported in part by NSF grants EAR-86-07324 (JDM), EAR-89-04042 (JDM and CDF) and EAR-91-17809 (JDM). Mike Carr is thanked for allowing us to obtain geochemical analyses in his DCP-AES laboratory at Rutgers University. Reviews by Jon Davidson and Charles Stern are gratefully acknowledged.

References

Baker DR, Eggler DH (1983) Fractionation paths of Atka (Aleutians) high-alumina basalts: constraints from phase relations. J Volcanol Geotherm Res 18:387–404

Baker DR, Eggler DH (1987) Compositions of anhydrous and hydrous melts coexisting with plagioclase, augite and olivine or low-Ca pyroxene from 1 atm and 9 kbar: application to the volcanic center of Atka. Am Mineral 72:12–28

Bingham DK, Stone DB (1972) Palaeosecular variations of the geomagnetic field in the Aleutian Islands. Geophys J R Astron Soc 28:317–335

Brophy JG (1987) The Cold Bay Volcanic Center, Aleutian Volcanic arc, II: implications for fractionation and mixing mechanism in calc-alkaline andesite genesis: Contrib Mineral Petrol 97:378–388

Brophy JG (1990) Andesites from northeastern Kanaga Island, Aleutians: implications for calc-alkaline fractionation mechanisms and magma chamber development. Contrib Mineral Petrol 104:568–581

Coats RR (1950) Volcanic activity in the Aleutian arc. US Geol Surv Bull 974(B):35–49

Coats RR (1952) Magmatic differentiation in Tertiary and Quaternary volcanic rocks from Adak and Kanaga Islands, Aleutian Islands, Alaska. Bull Geol Soc Am 63:485–514

Conrad WK, Kay RW (1984) Ultramafic and mafic inclusions from Adak Island: crystallization history and implications for the nature of primary magmas and crustal evolution in the Aleutian arc. J Petrol 25:88–125

Conrad WR, Kay SM, Kay RW (1983) Magmas mixing in the Aleutian arc: evidence from cognate inclusions and composite xenoliths. J Volcanol Geotherm Res 18:279–295

Cooper AK, Scholl DW, Marlow MS (1975) Plate tectonic model for the evolution of the eastern Bering Sea basin. Geol Soc Am Bull 87:1119–1126

Dall WH (1918) Reminiscences of Alaska volcanoes. Sci Monthly 7:80–90

Eggler DH (1972) Water-saturated and undersaturated melting relations in a Paricutin andestie and an estimate of water content in the natural magma. Contrib Mineral Petrol 34:261–271

Eggler DH, Burnham CW (1973) Crystallization and fractionation trends in the system andesite-H_2O–CO_2–O_2 at pressures to 10 kb. Geol Soc Am Bull 84:2517–2532

Feigenson MD, Carr MJ (1985) Determination of major, trace and rare-earth elements in rocks by DCP-AES. Chem Geol 51:19–27

Geist EL, Childs JR, Scholl DW (1987) Evolution and petroleum geology of Amlia and Amukta intra-arc summit basins, Aleutian ridge. Mar Petrol Geol 4:334–352

Geist EL, Childs JR, Scholl DW (1988) The origin of summit basins of the Aleutian ridge: implications for block rotation of an arc massif. Tectonics 7:327–341

Hein JR, McLean H, Vallier T (1984) Reconnaissance geology of southern Atka Island, Aleutian Islands, Alaska. US Geol Surv Bull 1609

Hildreth W, Lanphere MA (1994) Potassium–argon geochronology of a basalt-andesite-dacite arc system; the Mount Adams volcanic field, Cascade Range of southern Washington. Geol Soc Am Bull 106:1413–1429

Hooker PJ, O'Nions RK, Pankhurst PK (1975) Determinations of rare-earth elements in USGS standard rocks by mixed solvent ion exchange and mass-spectrometric isotope dilution. Chem Geol 16:189–196

Jaggar TA (1908) Journal of the technology expedition to the Aleutian Islands, 1907. Technol Rev 10:1–37

Kay SM, Kay RW (1994) Aleutian magmas in time and space. In: Plafker G, Berg HC (eds) The geology of Alaska: the geology of North America, vol G-1. Geol Soc Am, Boulder, CO, pp 687–722

Kay SM, Kay RW, Brueckner HK, Rubenstone JL (1983) Tholeiitic Aleutian arc plutonism: the Finger Bay pluton, Adak, Alaska. Contrib Mineral Petrol 82:99–116

Lindsley DH, Anderson DJ (1983) A two-pyroxene thermometer. Proceedings 13th Lunar and Planetary Science Conference. J Geophys Res 88:887–906

Linton JA (1993) Constraining the processes of magmatic evolution: perspectives from two volcanic centers. MSc Thesis, University of Wyoming, Laramie

Linton JA, Myers JD, Marsh BD (1993) Constraints of arc magma chamber processes as recorded by plagioclase phenocrysts: the Atka volcanic center, central Aleutian arc, Alaska. EOS Trans Am Geophys Union 74:348

Marsh BD (1980) Geology of northern Atka, Aleutian Islands, Alaska. Geol Soc Am Abstr Prog 12:476

Marsh BD (1982) The Aleutians. In: Thorpe RS (ed) Andesites: orogenic andesites and related rocks. Wiley, New York, pp 99–115

Marsh BD (1990) Atka. In Wood CA, Kienle J (eds) Volcanoes of North America. Cambridge University Press, New York, pp 29–31

Miller TP, McGimsey RG, Richter DH, Riehle JR, Nye CJ, Yount ME, Dumoulin JA (1998) Catalog of the historically active volcanoes of Alaska. US Geol Surv Open File Rep 98-582

Motyka R, Moorman M, Liss S (1981) Assessment of the thermal springs sites Aleutian arc, Atka Island to Becherof Lake – preliminary results and evaluation. Alaska Div Geol Geophys Surv Open-File Rep 144

Myers JD (1993) Plagioclase phenocryst compositions and zoning patterns: the Finch Cove Formation, Seguam volcanic center, central Aleutian arc. EOS Trans Am Geophys Union 74:348

Myers JD, Frost CD (1989) Trace and rare earth element constrains on the origin and evolution of Aleutian arc magmas. EOS Trans Am Geophys Union 70:721

Myers JD, Frost CD (1994) A petrologic re-investigation of the Adak volcanic center, central Aleutian arc, Alaska. J Volcanol Geotherm Res 60:109–146

Myers JD, Marsh BD (1987) Aleutian lead isotopic data: additional evidence for the evolution of lithospheric plumbing systems. Geochim Cosmochim Acta 51:1833–1842

Myers JD, Marsh BD, Sinha AK (1985) Strontium isotopic and selected trace element variations between two Aleutian volcanic centers (Adak and Atka): implications for the development of arc volcanic plumbing systems. Contrib Mineral Petrol 91:221–234

Myers JD, Marsh BD, Sinha AK (1986) Geochemical and strontium isotopic characteristics of parental Aleutian arc magmas: evidence from the basaltic lavas of Atka. Contrib Mineral Petrol 94:1–11

Nakagawa M, Wada K, Thordarson T, Wood CP, Gamble JA (1999) Petrologic investigations of the 1995 and 1996 eruptions of Ruapehu volcano, New Zealand: formation of discrete and small magma pockets and their intermittent discharge. Bull Volcanol 61:15–31

Nye CJ, Turner DL (1990) Petrology, geochemistry and age of the Spurr volcanic complex, eastern Aleutian arc. Bull Volcanol 52:205–226

Perfit MR, Brueckner H, Lawrence JR, Kay RW (1980) Trace element and isotopic variations in a zoned pluton and associated volcanic rocks, Unalaska Island, Alaska: a model for fractionation in the Aleutian calc-alkaline suite. Contrib Mineral Petrol 73:69–87

Romick JD, Perfit MR, Swanson SR, Shuster RD (1990) Magmatism in the eastern Aleutian arc: temporal characteristics of igneous activity on Akutan Island. Contrib Mineral Petrol 104:700–721

Scholl DW, Vallier TL, Stevenson AJ (1987) Geologic evolution and petroleum geology of the Aleutian ridge. In: Scholl DW, Grantz A, Vedder JG (eds) Geology and resource potential of the continental margin of western North America and adjacent ocean basins – Beaufort Sea to Baja California. Circum-Pacific Council Energy Res Earth Sci Series, Houston, TX, vol 6, pp 123–155

Sekine T, Katsura T, Aramaki S (1979) Water saturated phase relations of some andesites with application to the estimation of the initial temperature and water pressure at the time of eruption. Geochim Cosmochim Acta 43:1367–1376

Simkin T, Siebert L (1994) Volcanoes of the world. Geoscience, Tucson

Simons FS, Mathewson DE (1955) Geology of Great Sitkin Island, Alaska. US Geol Surv Bull 1028(B):21–43

Singer BS, Myers JD (1990) Intra-arc extension and magmatic evolution in the central Aleutian arc, Alaska. Geology 18:1050–1053

Singer BS, Myers JD, Frost CD (1992a) Mid-Pleistocene lavas from the Seguam volcanic center, central Aleutian arc: closed-system fractional crystallization of a basalt to rhyodacite eruptive suite. Contrib Mineral Petrol 110:87–112

Singer BS, Myers JD, Frost CD (1992b) Mid-Pleistocene basalts from the Seguam volcanic center, central Aleutian arc, Alaska: local lithospheric structures and source variability in the Aleutian arc. J Geophys Res 97:4579–4586

Singer BS, Pearce TH, Kolisnik AM, Myers JD (1993) Plagioclase zoning in mid-Pleistocene lavas from the Seguam volcanic center, central Aleutian arc, Alaska. Am Mineral 78:143–157

Singer BS, Thompson RA, Dungan MA, Feeley TC, Nelson ST, Pickens JC, Brown LL, Wulff AW, Davidson JP, Metzger J (1997) Volcanism and erosion during the past 930 k.y. at the Tatara-San Pedro complex, Chilean Andes. Geol Soc Am Bull 109:127–142

von Drach V, Marsh BD, Wasserburg GJ (1986) Nd and Sr isotopes in the Aleutians: multicomponent parenthood of island-arc magmas. Contrib Mineral Petrol 92:13–34

Wakita H, Rey P, Schmitt RA (1971) Abundances of the 14 rare earth elements and 12 other trace elements in Apollo 12 samples: five igneous and one breccia rocks and four soils. In: Proc 2nd Lunar Science Conf, pp 1319–1329

Winchester JW (1963) Rare earth chromatography using bis-(2-ethylhexyl) orthophosphoric acid. J Chromatogr 10:502–506